2011

EXAMINATION OF NAK-ASSOCIATED PROTEIN-1 (NAP1) HOMO AND HETERO-INTERACTIONS IN THE INTERFERON PATHWAY"

Richard Call
Virginia Commonwealth University

Department of Biochemistry and Molecular Biology
Virginia Commonwealth University

This is to certify that the thesis prepared by R. Jason Call entitled "EXAMINATION OF NAK-ASSOCIATED PROTEIN-1 (NAP1) HOMO AND HETERO-INTERACTIONS IN THE INTERFERON PATHWAY" has been approved by his committee as satisfactory completion of the thesis requirement for the degree of Master of Science

---

Dr. Jessica K. Bell

[Click here and type your Committee Member's Name and School Name.]

[Click here and type your Committee Member's Name and School Name.]

[Click here and type your Committee Member's Name and School Name.]

Dr. Sarah Spiegel, Chair of the Department of Biochemistry & Molecular Biology

---

Dr. Jerome Strauss, Dean of the School of Medicine

Dr. F. Douglas Boudinot, Dean of the School of Graduate Studies

[Click here and type the Month, Day and Year this page was signed.]

EXAMINATION OF NAK-ASSOCIATED PROTEIN-1 (NAP1) HOMO AND HETERO-INTERACTIONS IN THE INTERFERON PATHWAY

A thesis submitted in partial fulfillment of the requirements for the degree of Master of Science at Virginia Commonwealth University.

by

R. JASON CALL
B.S., UNIV. OF MARY WASHINGTON, 2006

Director: DR JESSICA K. BELL
ASSISTANT PROFESSOR, DEPARTMENT OF BIOCHEMISTRY & MOLECULAR BIOLOGY

Virginia Commonwealth University
Richmond, Virginia
JUNE 2011

Table of Contents

Page

List of Figures

Page

Abstract

EXAMINATION OF NAK-ASSOCIATED PROTEIN-1 (NAP1) HOMO AND HETERO-INTERACTIONS IN THE INTERFERON PATHWAY

By R. Jason Call, M.S

A Thesis submitted in partial fulfillment of the requirements for the degree of Master of Science at Virginia Commonwealth University.

Virginia Commonwealth University, 2011

Major Director: Dr. Jessica K. Bell, Ph.D.
Assistant Professor, Department of Biochemistry & Molecular Biology

Double stranded RNA (dsRNA), the genomic material of some viruses and a replication intermediate in others, is recognized by multiple signaling receptors that initiate the anti-viral response[1]. Viruses have developed mechanisms to circumvent the anti-viral response by targeting components of the signaling pathway. An example of one such pathway is the TLR3 signaling pathway, which contains a kinase complex that activates interferon regulatory factor 3 (IRF3), leading to production of type I interferons. The kinase complex consists of a scaffold protein, NAK-associated protein 1 (NAP1), and two kinases, TANK-binding kinase 1 (TBK-1) and IκB kinase epsilon (IKKε). A fourty residue sequence in NAP1 was discovered that mediated its interaction with TBK1 and IKKε, termed the kinase binding domain (KBD)[1]. However, the function of NAP1 in mediating kinase activation is unknown and understanding this is the long-term goal of this

project. The goal of this thesis was to test the dependency of NAP1's dimeric structure on mediating interactions with the kinases. Biochemical characterization of recombinant targets was completed using size-exclusion chromatography (SEC) and NAP1 KBD WT eluted as a dimeric species. CFP/YFP/Alexa Fluor 546 fusion proteins of the NAP1 KBD and scaffold binding motif (SBM) of the kinases, TBK-1 and IKKε, were generated to assess interactions using fluorescence resonance energy transfer (FRET). NAP1 KBD directly interacts with TBK1 and IKKε, with low micromolar affinity *in vitro*. Mutagenesis was attempted to identify the residues necessary for NAP1 dimerization and any effect dimerization may have on kinase recognition. This thesis shows data to support that NAP1 KBD forms stable homo-oligomers and directly interacts with a small C-terminal portion of TBK1 and IKKε.

Chapter 1. Introduction

Protein-protein interactions are responsible for a great variety of cellular functions. In the most basic sense, a protein-protein interaction occurs when two proteins come together and form some type of interaction. Protein-protein interactions are a common form of communication in signaling. For instance, when two proteins bind one another, activation of a different protein, post-translational modification, or recruitment of other proteins can occur. This recruitment process can be performed by a class of proteins known as scaffold proteins, which act as docking stations for the formation of a protein complex, which can lead to production of type I inteferons (IFNs), Nuclear Factor-KappaB (NF-kB), as well as, downstream signaling to chemokines and cytokines, to destroy invading pathogens.

Over the last several decades, pathogens have acquired the means to evade anti-viral signaling[2] or block receptor recognition[3] as a means to promote pathogen survival and replication. Viral proteins are known to interact with components of the anti-viral signaling response and can disable the host from sequestering the pathogen's genomic material, as well as, inhibit phosphorylation-mediated signaling and block protein complex formation. Therefore, structurally characterizing the domains involved in these interactions and how they may form complexes with other proteins is vital to understanding how these interactions mediate cellular processes and how to counter viral evasion.

1.1 The Innate Immune System

The immune response is comprised of two parts: innate and adaptive immunity, both are essential for a complete immune response. The innate immune response is the first line of defense, against invading pathogens, with dendritic cells constantly sampling cells, both self and non-self alike, to monitor the body for an infection. When an infected cell is spotted this is where the macrophages come in to do their work. Macrophages are known for engulfing foreign cells, via a process called phagocytosis, that are then digested internally and cause the release of cytokines and chemokines to transmit a local inflammatory response and prevent the spread of the invading pathogen to nearby cells[4]. This is one of the two main functions of the innate immune response, with the other function being the activation of the adaptive immune response.

For example, the presence of a viral pathogen often leads to the production of interferon. Interferons are aptly named because of their ability to "interfere" with invading pathogen's replication process[4]. Type-I interferons', such as IFN-α and IFN-β, role is to mediate the activation of cytokines and chemokines to help prevent pathogen replication in infected cells. Additionally, this activation can cause upregulation of major histocompatibility complex (MHC) molecules on uninfected cells[5]. There are two classes of MHC molecules: class I and class II molecules; where class I molecules present peptides derived from cytosolic proteins. Class II molecules, which are only found on a few specialized cell types, such as macrophages, dendritic cells and B cells, present peptides derived from extracellular proteins. However, both types of molecules present

peptides derived from infecting pathogens for recognition by T cells, to help clear the infection, as part of the adaptive immune response.

Mainly antibodies and lymphocytes carry out the adaptive immune response, which allows for a specific response to the invading pathogen. However, it is the connection between the innate and adaptive response that is critical to fighting off the viral infection.

Nonetheless, the innate and adaptive immunity responses require different recognition sources for activation. While the adaptive response relies on an antigen-specific response and the innate immune response is dependent on recognition of a set of evolutionarily conserved pathogen elements, otherwise known as pathogen-associated molecular patterns (PAMPs)[5]. These PAMPs form a direct interaction with a class of host receptors known as pattern recognition receptors (PRRs) that mediate the innate immune response[5]. The recognition of PAMPs instead of self is what differentiates between an appropriate immune response and an over-active or autoimmune response, which can cause a variety of illnesses.

For everything the immune response does well there are also a few drawbacks, the innate immune system can also lose its ability to distinguish between self and non-self, targeting endogenous cells as infectious agents leading to autoimmune diseases such as autoimmune diabetics, liver disease and lupus nephritis, a kidney autoimmune disease[6]. Furthermore, the innate immune response may also over-respond to non-infectious agents, creating symptoms of what are commonly referred to as allergies. While seasonal allergies are generally a nuisance, allergic reactions to things such as nuts or dairy can be fatal[7]. Furthermore, over the last several decades pathogens have acquired the means to evade

receptor recognition or block anti-viral signaling as a means to promote pathogen survival and replication (2,3).

1.2 Pattern Recognition Receptors

The immune system response and more specifically the innate immune response varies depending on the evolutionarily conserved pathogen element, or PAMP, that is recognized. This allows the human body to ignore self-molecules while focusing solely on finding, containing and destroying foreign molecules[2]. The wide range of PRRs allows the human body to recognize an array of structural distinct bacterial and viral particles. There are three localization types of PRRs: membrane-bound, cytoplasmic and secreted. The membrane-bound PRRs are further classified into three subgroups: receptor kinases, which originated in plants, and the toll-like receptors (TLRs) and the mannose receptor, which are both found in humans[4].

The mannose receptors, primarily present on the surface of innate immune cells, recognize and bind to mannose repeats of infectious agents[2]. This activation triggers endocytosis and phagocytosis of the invading pathogen. As previously described, the engulfing of the invading particle and its subsequent digestion allows for peptide presentation of the foreign molecule via MHC molecules, which lead to eventual targeting and killing by the cytotoxic T cells.

Recognition of both extracellular (TLR1,2,4,5,6,10) or endosomal (TLR3,7,8,9) PAMPs, including bacterial lipoproteins (i.e LPS) and DNA-based ligands (i.e dsRNA), is mediated by an array of transmembrane proteins known as TLRs. Toll-like receptors were first discovered in Drosophila and are known to trigger a series of mechanisms leading to the synthesis and secretion of cytokines and transcription factors that are crucial to the development of innate and adaptative immune responses. In humans, there are currently eleven such receptors (TLR1-11). Interaction of TLRs with their specific PAMP induces a wide variety of signaling cascades consisting of NF-κB and type I interferon signaling, MAP kinase pathways and apoptosis and autophagy. These pathways result in secretion of pro-inflammatory cytokines and chemokines, as well as, transcription factors necessary to activate the adaptive immune response and generate a complete immune response[3].

1.3 Activation of type I Interferons and NF-κB signaling

One such PAMP, double stranded RNA (dsRNA), the genome of some viruses, can be recognized by a variety of receptors. TLR3, retinoic acid inducible gene-1 (RIG-I), melanoma differentiation associated gene 5 (MDA5) and dsRNA-dependent protein kinase receptor (PKR) all bind dsRNA. However, these receptor have different cellular localization, which leads to different downstream signaling. TLR-3 is located in the endosome, whereas RIG-I, MDA-5 and PKR are located in the cytoplasm[6]. For example, when TLR3 binds dsRNA, activation can lead to three distinct signaling pathways,

resulting in production of type I Interferons or NF-kB and a third involving the cleavage of caspase 8, which leads to apoptosis (Figure 1).

In the pathway leading to production of type I Interferons, the signaling cascade is initiated when Toll/Interleukin 1 receptor (TIR)-domain-containing adapter inducing-interferon-β (TRIF) is recruited to TLR3's interior-signaling domain. TRIF via tumor necrosis factor receptor-associated factor 3 (TRAF3) interacts with a scaffold protein to mediate downstream signaling. Currently, two scaffold proteins; Nak-associated protein 1 (NAP1) and Similar to NAP1 TBK1 adaptor (SINTBAD) have been identified. The scaffold protein(s) act as a docking site for two kinases, TRAF family member-associated NFKB activator (TANK)-binding kinase-1 (TBK1) and IκB kinase epsilon (IKKε). Together, the scaffold protein(s) and kinase(s) form a kinase complex. The exact make-up of the kinase complex is not fully understood. The activated kinases can phosphorylate interferon-regulatory factor 3/7 (IRF3/7) allowing these transcription factors to dimerize and traffic to the nucleus to initiate transcription of the interferon-β gene (IFN-β). Upon transcription and release of IFN-β, it can bind to the downstream interferon alpha-receptor 1/2 (IFNAR1/2), which triggers the JAK/STAT pathways and leads to activation of a host of interferon-stimulated genes. This is the end result of the interferon response that allows for halting the viral replication of the invading pathogen and hopefully apoptosis of the viral-infected cells.

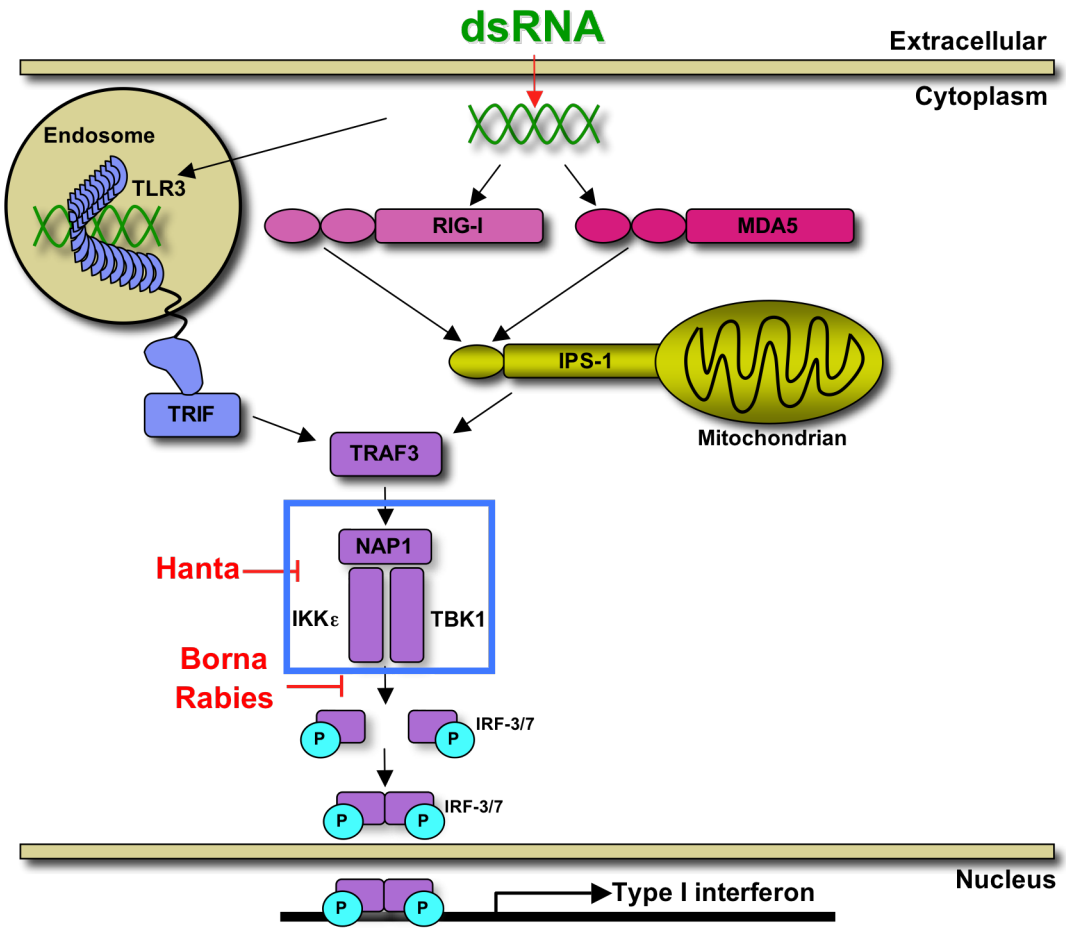

Figure 1. *Cartoon diagram of the TLR3 signaling pathway leading to type I interferon production.* The kinase complex of interest in our studies is enclosed in the blue box. Viruses which target this kinase complex for subversion, and thus immune evasion, are shown in red typeface. TRIF, Toll/IL-1 domain containing adaptor inducing interferon-b; TRAF3, Tumor necrosis factor receptor associated factor 3; TANK, TRAF-associated activator of NF-kB; NAP1, NAK-associated protein 1; TBK1, TANK binding kinase 1; IKKe, IkB kinase epsilon.

In addition to the IRF3/7 pathway, TRIF can also initiate the nuclear factor- kappa B (NF-κB) essential modulator (NEMO/IKKγ) pathway, which leads to the formation of a kinase complex, as well. Despite the formation of a kinase complex, like the IRF3/7 pathway, these pathways have some distinct differences. NEMO causes recruitment of two different kinases, Iκ-B kinase beta (IKKβ) and Iκ-B kinase alpha (IKKα), to form a kinase complex (Figure 2A). A partial crystal structure of the kinase complex[8] has been solved; involving the minimal kinase-binding domain (KBD) of NEMO, NEMO44-111, which structurally is a dimer, binding two identical copies of a peptide that was generated from a conserved NEMO-binding domain sequence found in the two kinases, IKKα and IKKβ, sequence (Figure 2B). This particular conserved region is not present in the TBK1/IKKε kinase complex. However, a unique conserved site, at the C-terminus, has been discovered in our lab via sequence alignments.

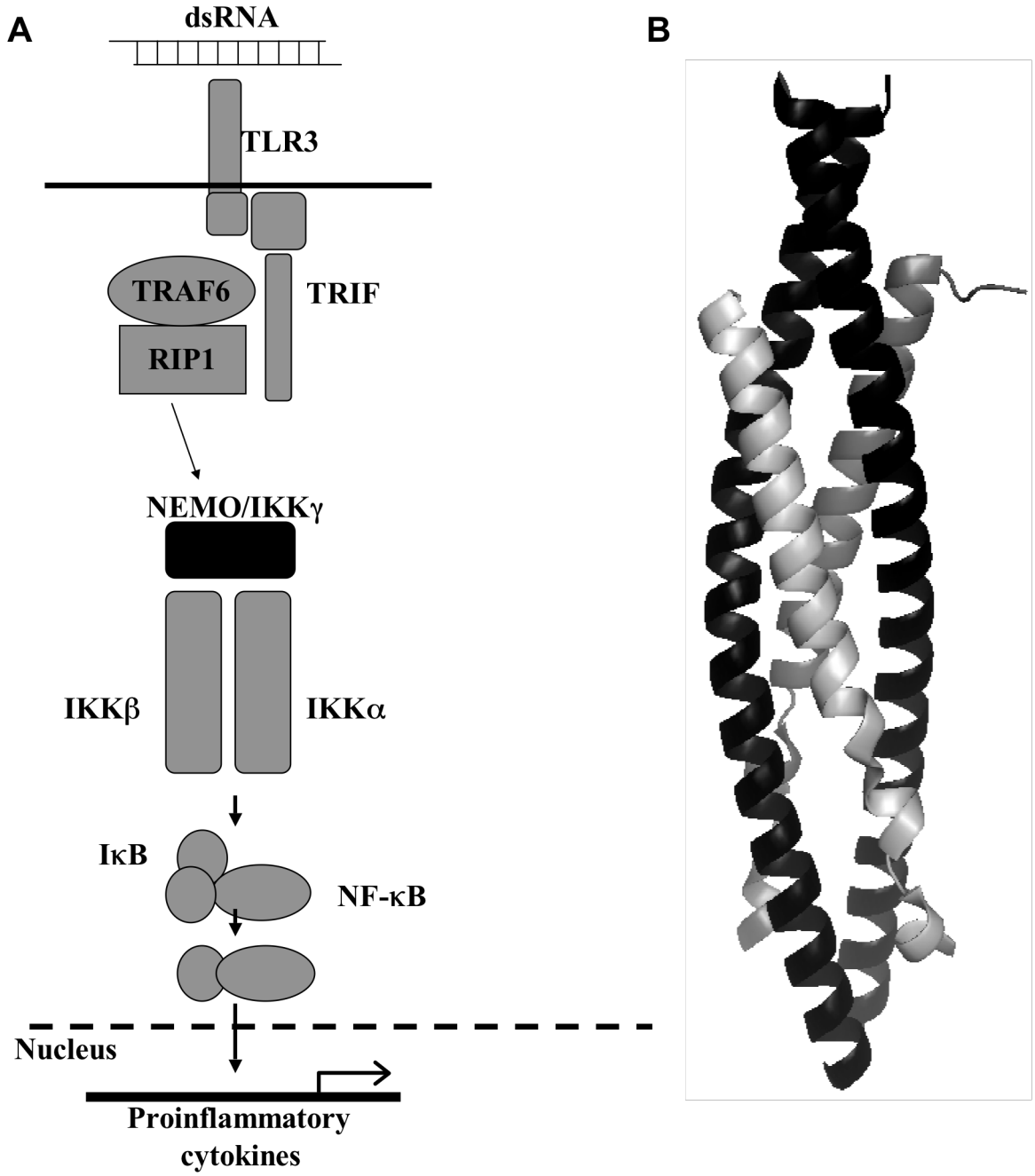

Figure 2. *Cartoon diagram of the TLR3 signaling pathway leading to NF-κB production.* **A)** Recruitment of TRAF6 and RIP1 to TRIF allow for downstream signaling and formation of a kinase complex comprised of a scaffold protein, NEMO/IKK γ, and two kinases, IKKα and IKKβ, which phosphorylate IκB allowing for NF-κB production. **B)**Structure of the kinase complex, with dimeric NEMO (green) forms a binding pocket for two copies of IKK peptides (in different shades of blue) to bind inside. TRIF, Toll/IL-1 domain containing adaptor inducing interferon- β; TRAF6, Tumor necrosis factor receptor associated factor 6; RIP1, Receptor-Interacting Protein 1; NEMO/IKK γ, NF-kappa-B essential modulator/I κB kinase γ; IKKα, IκB kinase α; IKKβ, IκB kinase β.

1.4 NAP1-TBK1 mediated type I Interferon Signaling

Both the NAP1 and SINTBAD scaffold proteins, also have a conserved site, that have been shown to recognize the kinases, TBK1 and IKKε[1] (Figure 3). NAP1 has also been shown to bind SINTBAD; questioning whether it functions independently with the kinases or with the aid of another scaffold protein(s)[1]. These protein-interaction domains are used to form large molecular weight protein interaction networks (PINs). In fact, both NAP1 and TBK1 were components of high molecular weight complexes in TLR3 unstimulated HeLa cells[9]. In addition, both of these scaffold proteins have multiple predicted coiled-coil domains, which are rod-like alpha helices that are known to mediate protein-protein interactions.

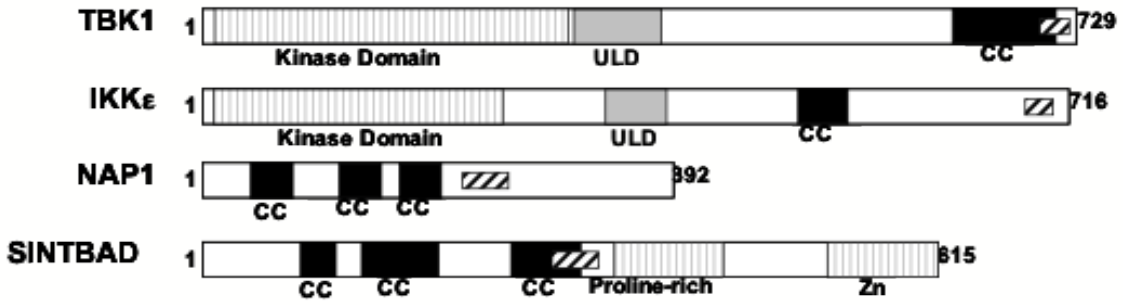

Figure 3. *Cartoon diagram of kinase complex components' domain structure.* TBK1, TANK binding kinase 1; IKKε, IkB kinase epsilon; NAP1, NAK-associated protein 1; SINTBAD, Similar to NAP1 TBK1 adaptor domain; SIKE, suppressor of IKKε; CC, coiled coil; Zn, zinc finger motif. Striped boxes indicated kinase-binding domain (KBD) or scaffold-binding motif (SBM).

The hypothesis is that NAP1's protein domains have interaction specificity that has a direct impact on its signaling (Figure 4). This hypothesis suggests that the CC domain region of NAP1, residues 1-200, which highly alpha helical in structure, mediate its ability to homo-dimerize. This homo-dimerization brings the kinase-binding domains in close proximity that they have also been shown to homo-dimerize, but more importantly is the hetero-interactions they form with the kinases' scaffold-bindind motif[1]. NAP1's ability to behave as a dimer, may be necessary for NAP1's kinase-binding domain's hetero-interactions with the kinase, which is necessary for downstream signaling and production of type I IFNs. The end result being to better understand the TLR3-dependent PIN and how it may be manipulated to control disease states.

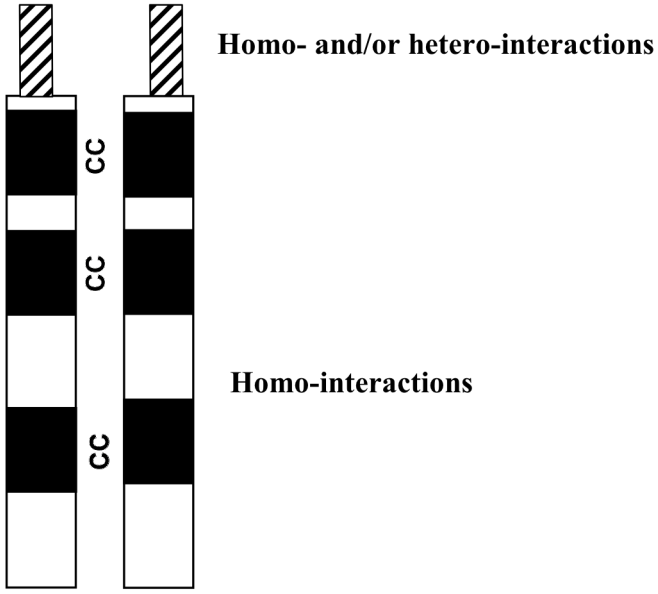

Figure 4. *NAP1 forms homo- and hetero-interactions.* The following diagram depicts the homo-interactions of NAP1 protein domains. Shows the possible confirmations of the dimeric NAP1CC (1-200), shown as black boxes, and NAP1 KBD (216-255), shown in boxes and dashed lines,

Chapter 2. Materials and Methods

2.1 Bacterial Production of Recombinant Protein domains

All bacterial constructs discussed below were DNA sequence confirmed and then transformed into BL21 Codon Plus per manufacturer's protocol (Stratagene). For protein expression, 50ml cultures were grown at 37 degrees Celsius and 200rpm in Lennox Broth (LB) media and ampicillin overnight and used to inoculate media for large-scale protein expression per manufacturer's protocol. Cells continued to grow at 37 degrees Celsius for four to six hours (2.1.2) or at 20 degrees Celsius overnight (2.1.1 and 2.1.3), before harvesting. Cells were harvested by centrifugation, 8000 rpm for 20 minutes, and cell pellets were stored at -80°C.

2.1.1 CFP/YFP Tagged Protein Purification

All constructs used for FRET assays were made prior to starting on this project (CFP NAP1 KBD, CFP, YFP, YFP TBK1 SBM, GST TBK1 SBM and GST IKKε SBM). However, all CFP and YFP fluorescent-tagged constructs were found to be dimeric. Quikchange mutagenesis kits (Stratagene) that employed standard molecular biology and polymerase chain reaction (PCR) techniques were used to generate monomeric fluorescent-tagged (A206K) constructs as per manufacturer's protocol. An additional mutation was performed to change YFP constructs to Citrine variants (Q69M). Constructs made include:

mCFP NAP1 KBD, mCFP, mCitrine TBK1 SBM, mCitrine. All CFP/YFP constructs are in pET15b, a bacterial expression vector that includes an N-terminal 6xHistidine tag for immobilized metal affinity chromatography purification following expression. Additional mutants were made to the mCFP NAP1 KBD to test their effects on dimer stability.

For purification, cell pellets were resuspended in Binding Buffer (20mM PO_4 (pH 8), 500mM NaCl, 2mM $MgCl_2$ and 1mM beta-mercaptoethanol (βME) including 1 protease inhibitor tablet) and purified per manufacturer's protocol (Qiagen). Cell lysis was performed, on ice, using a Avestin C3 emulsifier instrument. Passage was performed 3-4 times at 15K-20K psi. Run program "1ml Histrap cfp proteins RJC" while collecting 1ml fractions using the AKTA system at 4 degrees Celsius. This program washes the column with 20 CV of 100% Binding Buffer, 10 CV gradient from 0 to 10% Elution Buffer, washes with 5 CV of 10% Elution Buffer, 25 CV gradient from 10 to 100% Elution Buffer and washes with 10 CV of 100% Elution Buffer. Peak fractions are analyzed by SDS-PAGE gel analysis for target protein and visualized with coomassie blue stain. Histrap column is regenerated per manufacturer's instructions (Qiagen).

2.1.2 Purification and Refolding of Recombinant Protein

NAP1CC, the first 200 amino acids, was expressed as insoluble material. To purify the insoluble NAP1CC, the insoluble protein was extracted from the bacterial pellet using 6M GuHCl. Purification by nickel-nitrilotriacetic acid (Ni-NTA) resin was completed

following the manufacturer's instructions for batch purification under denaturing conditions (Qiagen).

2.1.3 Glutathione-S-Transferase fusion tagged construct purification

The GST fusion proteins are in the pGEX-4T1 vector, a bacterial expression vector that includes a Glutathione-S-transferase tag for affinity chromatography purification following expression, per manufacturer's protocol (GE Healthcare). Quikchange mutagenesis kits (Stratagene) that employed standard molecular biology and polymerase chain reaction (PCR) techniques were used to mutate a valine to a cystine residue at the N-terminus of the TBK1 SBM peptide to allow for linkage with the Alexa-Fluor 546 molecule.

2.2 Baculovirus Production of Recombinant kinases

2.2.1 pFastbac Construct Preparation

Dr. Katherine Fitzgerald (UMass-Amherst) kindly provided a pFASTBAC vector containing an N-terminal FLAG-affinity tag followed by the TBK1 gene. The IKKε gene was later cloned into the same expression vector using primers that contained unique restriction sites (5' BamHI and 3' SpeI) for the pFASTBac vector multiple cloning site.

2.2.2 Bacmid Generation

Sequence confirmed IKKε pFASTBac and TBK-1 pFASTBac DNA was transformed into DH10Bac competent cells per manufacturer's protocol (Invitrogen).

2.2.3 Bacmid DNA Purification

Overnight cultures of pFASTBac transfected DH10Bac cells were pelleted at 14.000 *x g* for 10 minutes at room temperature. DNA was extracted via Qiagen mini-prep kit, but modified to the Bac-to-Baculovirus Invitrogen protocol.

2.2.4 Insect Cell Virus Propagation

All insect cell work was carried out using sterile technique in a laminar flow hood, biosafety cabinet IIA. Sf-9 cells were cultured in Hyclone SF-X Media (Thermo Scientific). For bacmid transfection, again Bac-to-baculovirus protocol was followed (Invitrogen).

2.2.5 Determining Viral Titer

Viral titer plaquing assays to determine viral titer were completed as per Bac-to-Bac

instruction manual (Invitrogen). Sf-9 cells were plated at a density of 1.0 x 10^6 cells/well in two 6-well culture plates. Cells were allowed to adhere at room temperature for 1 hour. Meanwhile, serial dilutions of P2 viral stock were made from 10^{-1} to 10^{-8} fold dilutions in SF-X media. Cell adherence is confirmed before removal of media. Media is then removed from wells and replaced with 1 ml of diluted virus (from 10^{-3} to 10^{-8}). Each dilution of virus was done in duplicate, along with a control (no viral addition). Wells were allowed to incubate with virus for 1 hour at room temperature on an orbital shaker, slow speed. Low melting temperature agarose (4 %, 10 ml) and 30 ml of SF-X media were warmed to 37°C, and then combined to make plaquing media. After incubation, plates were returned to hood, and plaquing media was allowed to cool but not thicken to prevent cell death. Viral dilution media was removed from cells, and 2ml of plaquing media (cooled slightly) was added to wells, slow addition along the wall of the well. Plaquing media was allowed to set for 10-20 minutes with the lid slightly cracked to avoid condensation. Plates were placed in a virus-specific incubator at 27°C for 4 days. After four days, 1 ml neutral red staining solution, consisting of 1% agarose, 62.5 μg/ml neutral red stain in SFX media, was added to each well to stain the plaques. Agarose was allowed to harden and plates were returned to humidified incubator for 2-3 days. Plaques (cleared areas) were counted for each well, and averaged for each dilution. Titer was calculated by:

Titer (pfu/ml) = (# of plaques) x (dilution factor) x (1ml of inoculum/well)

Viral stocks were replenished using the protocol described for P2 viral stock and titred as

described above.

2.2.6 Baculovirus Expression and Protein Purification

Sf9 cells cultured in suspension were infected with FLAG-tagged TBK1 or IKKε incorporated baculovirus as described in the literature[10] to express the kinases. The cells were infected at a cell density of 1.5 x 10^6 cells/ml with a multiplicity of infection (MOI) of three. Cells were harvested fourty-eight hours post-infection and then lysed by emulsification (Avestin Emulsiflex C3) at 20,000 psi. The kinases were purified from clarified cell lysates by anit-FLAG M2-agarose affinity column chromatography as per manufacturer's protocol (Sigma) and eluted using 0.34mg/ml of FLAG peptide. SEC was performed to remove the FLAG peptide from the kinase solution. Fractions containing kinase were concentrated, where the concentration was determined by Biorad assay with a 1000-fold dilution of protein to Biorad reagent. Kinase was stored at -80 degrees Celsius in kinase storage buffer: 20mM Tris-HCl (pH 7.6), 150mM NaCl, 0.1% Nonidet P-40, 10% glycerol, 20mM NaF, 20mM β-glycerophosphate, 1mM EDTA, 5mM DTT, 1 EDTA-free protease inhibitor tablet, 0.1%BSA as detailed[10].

2.3 mCFP NAP1 KBD Protein Interactions

2.3.1 Molecular Modeling

The Protein Databank (PDB) was used to find a related structure of a coiled-coil domain protein. The crystal structure of the C-terminal region of striated muscle alpha-tropomyosin (1KQL) was used as a template and all the residues were mutated to match the target sequence (NAP1 216-255) using Pymol. Once mutated the structure was energy minimized using a program called PHIEX. Following minimization, two copies of the structure were sent for analysis for docking interactions, using a program called ZDOCK, which holds one structure fixed and rotates the other structure to it and outputs possible interactions arrangements for the pair. Possible complexes are scored and ranked based on shape complementarity, desolvation, electrostatics and free energy change.

2.3.2 Size Exclusion Chromatography

Elutions from Ni-NTA purification and FLAG purification were separated on a Superdex™ 200 16/60 prep grade column (GE Healthcare) pre-equilibrated in 20 mM HEPES, pH 7.5, 150 mM NaCl and 1 mM βME (Ni-NTA purifications) and 20 mM HEPES, pH 7.5, 500 mM NaCl, 5% glycerol and 1 mM DTT (FLAG purifications), respectively. Elution volumes at peak maximums were converted to K_{av} and compared to a standard curve (K_{av} versus log molecular weight) based upon globular standards of known molecular weights (previously derived) using this equation:

$$K_{av} = \frac{\text{elution volume} - \text{void volume}}{\text{total volume} - \text{void volume}}$$

Peak fractions for all runs were analyzed by 10% SDS-PAGE and visualized with coomassie blue stain.

2.3.3 Fluorescence Resonance Energy Transfer

The kinase-binding domain (KBD) of NAP1 was linked to cyan fluorescent protein (CFP) and the kinase's interaction motif was fused to citrine fluorescent protein (CitFP). Fluorescence resonance energy transfer (FRET) between CFP and CitFP was measured to assess interactions, by exciting at 430nm and following emission at 530nm. Alternatively, the kinase's interaction motif was conjugated to the fluorophore Alexa Fluor 546 (AF546). Again, examining the interactions, by exciting at 430nm and following emission at 570nm. Fluorescence measurements were performed using a Fluorescence Spectrophotometer (instrument name). The excitation and emission bandpass were both set at a value of 2nm. Emission spectra were collected from a range of 450nm to 600nm with data points being collected every nm and each spectrum was collected three times and averaged.

2.4 Purification and Isolation of IKKε SBM-546 labeling

Upon successful purification of the GST IKKε SBM protein it was coupled with mCFP NAP1 KBD were examined for hetero-interactions via fluorescent resonance energy transfer (FRET). Prior to completing the FRET experiments, IKKε SBM was cleaved,

using 10U thrombin/mg target protein, to separate the peptide from the GST-tag. Upon successful cleavage of the fusion protein, free GST-tag is allowed to bind to Glutathoine-S-transferase 4B resin and thrombin is allowed to bind benzamidine resin, thus, leaving only the IKKε peptide in the supernatant. Upon isolation of the IKKε peptide, verification analysis using mass spectrometry (MS) was performed by Jimmy Marion (of the Bell lab). After confirmation of successful peptide isolation the peptide is labeled using a small molecule fluorophore, Alexa-Fluor 546, per manufacturer's protocol (Invitrogen). This process is verified using MS that was performed by Jimmy Marion (of the Bell lab).

2.5 Protein Concentration

Protein concentrations were determined by BioRad protein assay (BioRad) as per manufacturer's protocol. As needed, protein samples were concentrated by ultrafiltration (Amicon Ultrafiltration Units).

2.6 Circular Dichroism and Thermal Melt

NAP1CC sample were dialyzed into 100 mM sodium phosphate, pH 7, 150mM NaCl, 5% glycerol overnight at 4°C. Dialysis buffer was retained as a buffer blank. CD spectra (190-300nm) were collected on a Jasco 720 Circular Dichroism Spectrometer via collaboration with Dr. Ellis Bell at the University of Richmond. Five individual spectra

collecting data points every 0.1nm were collected averaged and Savitz-Golay smoothed using the Jasco Spectra Manager software.

Thermal melt data were collected from 4°C-90°C at A_{222nm}. Data was collected at 1 degree Celsius intervals. Data were Savitz-Golay smoothed using the Jasco Spectra Manager software.

2.7 Analytical Ultracentrifugation (work done by R. Ghirlando)

Sedimentation velocity experiments were completed by R. Ghirlando (NIH). Data was collected at 4 degrees Celsius, 55K rpm and various protein concentrations (33-134μM) 0.435 to 3.49mg/ml in 20mM HEPES (pH 7.5), 150mM NaCl and 1mM βME. Dialysis buffer was retained as a buffer blank. Protein concentrations were determined by Biorad assay (2.4). Data was analyzed in terms of a continuous c(s) sedimenting species, which provides a concentration profile (c) for each sedimenting species with a sedimentation coefficient s. Data was fitted using SEDFIT program. Plots were completed showing the concentration (in terms of A_{280}) as a function of best fit (s20w).

Chapter 3. Results

Toll-like receptor 3 (TLR3) is stimulated by dsRNA, the viral genomic material in some viruses or a viral replication intermediate in others. This stimulation initiates signaling cascades that lead to the activation of nuclear factor kappa B (NF-κB) and IRF3/7. Within the TLR3 signaling cascade that activates interferon regulatory factor 3/7 (IRF3/7), two scaffold proteins, Nak-associated protein 1 (NAP1) and Similar to NAP1-TBK1 adaptor (SINTBAD), can recruit and bind two kinases, TRAF family member-associated NFKB activator (TANK)-binding kinase 1 (TBK1) and IkB kinase epsilon (IKKε), which phosphorylate IRF3/7 and promote production of type I interferons (IFNs), NF-kB, as well as, downstream signaling to chemokines and cytokines, to destroy invading pathogens.

3.1 Nak-associated protein 1 (NAP1) interactions via coiled-coil (CC) domain

3.1.1 Expression and Purification

Full-length NAP1 was expressed as insoluble material via bacterial expression. So, quikchange mutagenesis was performed to truncate the NAP1 full-length protein to contain only its first 200 amino acids, NAP1CC (residues 1-200) (Figure 5). This construct was generated in pET15b, a bacterial expression vector that includes an N-terminal 6xHistidine tag for immobilized metal affinity chromatography purification following expression.

However, NAP1CC was also expressed as insoluble material. To purify the insoluble NAP1CC, the bacterial pellet was resuspended and the protein unfolded using 6M-guanidine hydrochloride (GuHCl). Purification by nickel-nitrilotriacetic acid (Ni-NTA) resin was completed following the manufacturer's instructions for batch purification under denaturing conditions (Qiagen). NAP1CC was eluted in 5ml aliquots with 0.5M imidazole in binding buffer. Purity was assessed by separation by SDS-PAGE and coomassie stain (Figure NAP1CC purification)

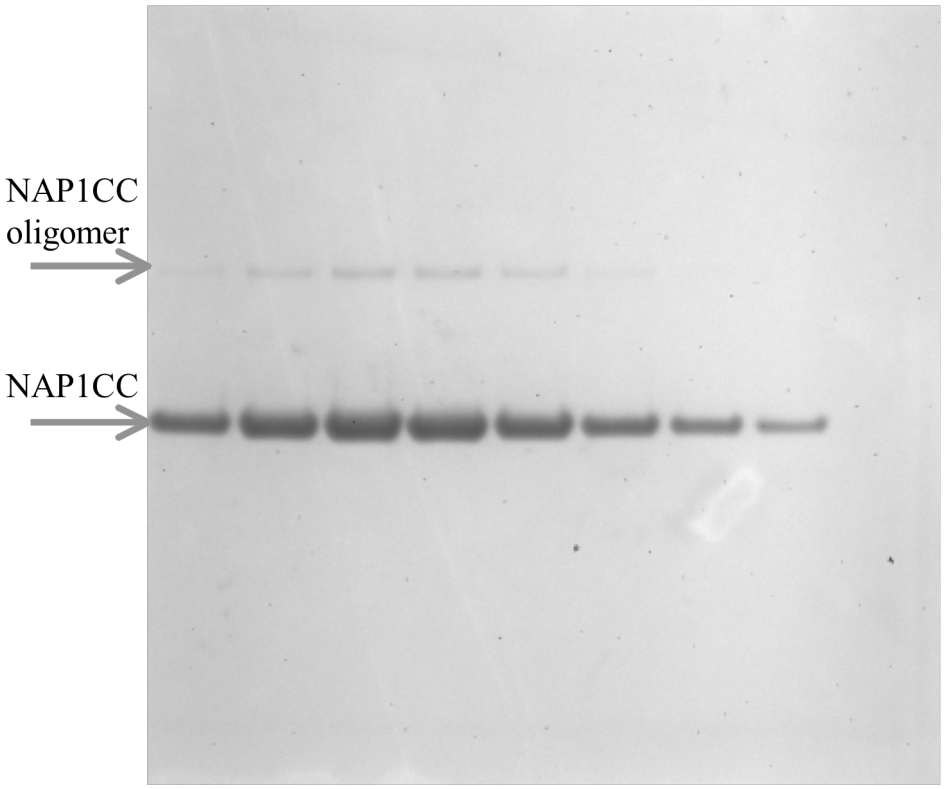

Figure 5. *Successful purification of refolded NAP1CC.* Samples were run on 10% Bis-Acryl SDS-PAGE gels showing recombinant protein purification from SEC fractions. Gray arrows indicate full-length protein. There is also evidence of higher-order oligomeric species No evidence of degradation. Abbreviations the same as in Figure 1.

3.1.2 Circular Dichroism and Thermal Melt

Successful refolding was assessed by examining secondary structure content using circular dichroism (CD). A UV-Vis scan was collected, via CD, and can detect secondary structures motifs, such as alpha helices and beta sheets. NAP1CC, which encompasses only the CC region, should contain almost exclusively alpha helical secondary structure. The CD spectrum of NAP1CC shows two negative ellipticity peaks at 222 and 208nm (Figure 6A), which is indicative of alpha helical secondary structure. Furthermore, the thermal melt data (Figure 6B) indicates a stepwise loss of helical content as the temperature is increased. This suggests that NAP1CC forms higher order oligomers and that as the temperature is increased the monomers dissociate and eventually the individual alpha helices are separated, as well.

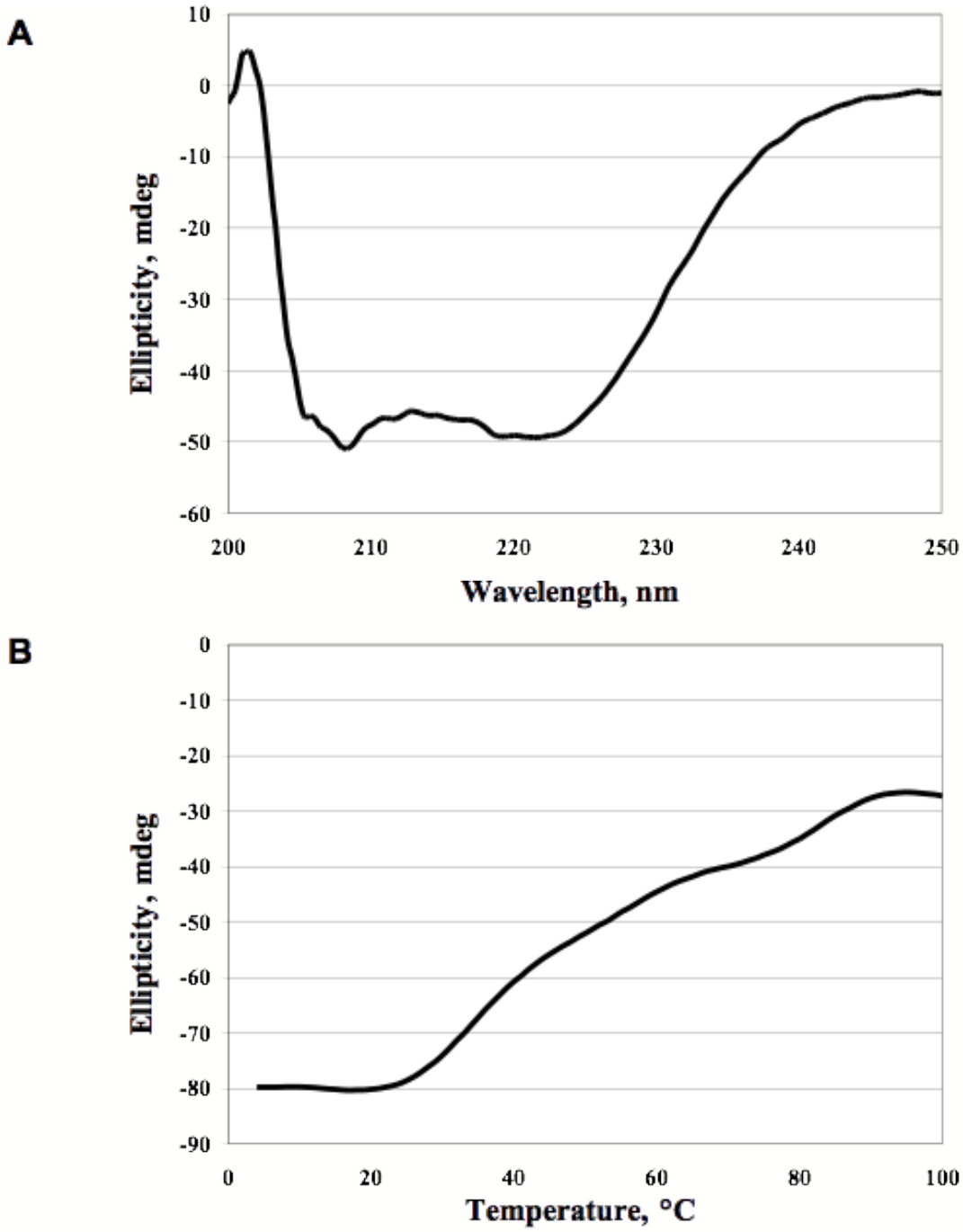

Figure 6. *CD confirms alpha helical content of NAP1CC.* **A)** CD Spectrum of NAP1CC (0.1 mg/ml in 0.1 M $NaPO_4$, pH7, 5% glycerol) from 200-250nm shows negative ellipticity at 208 and 222 nm consistent with alpha helical content. **B)** Thermal denaturation, measured as a function of ellipticity at 222nm, reveals multiple states of unfolding.

3.1.3 Size-exclusion chromatography (SEC)

To access the oligomeric state of the NAP1CC protein (Figure 7A), SEC experiments were completed. SEC separates proteins in the liquid phase as a function of their ability to interact with a column matrix. Larger proteins elute first because of their inability to interact with the matrix while smaller proteins elute later. An approximate molecular weight of an eluted species can be determined based upon the elution pattern of globular protein with well-characterized molecular weights. NAP1CC was tested at three different concentrations: 0.1mg/ml, 1.2mg/ml and 20mg/ml (Figure 7B). All of the experiments were completed on a Superdex 200 column (GE) in the following buffer: 20 mM HEPES (pH 7.5), 150mM NaCl, 5% glycerol and 1mM DTT.

The elution profile of NAP1CC indicated the major species eluted as a hexamer (Figure ?) with a minor peak eluting as a 12-mer. CC domains are rod-like structures, which tumble in solution with a larger radius than a globular protein with similar molecular weight. Therefore, while SEC is useful in determining purity of these types of protein samples, it may only approximate the molecular weight.

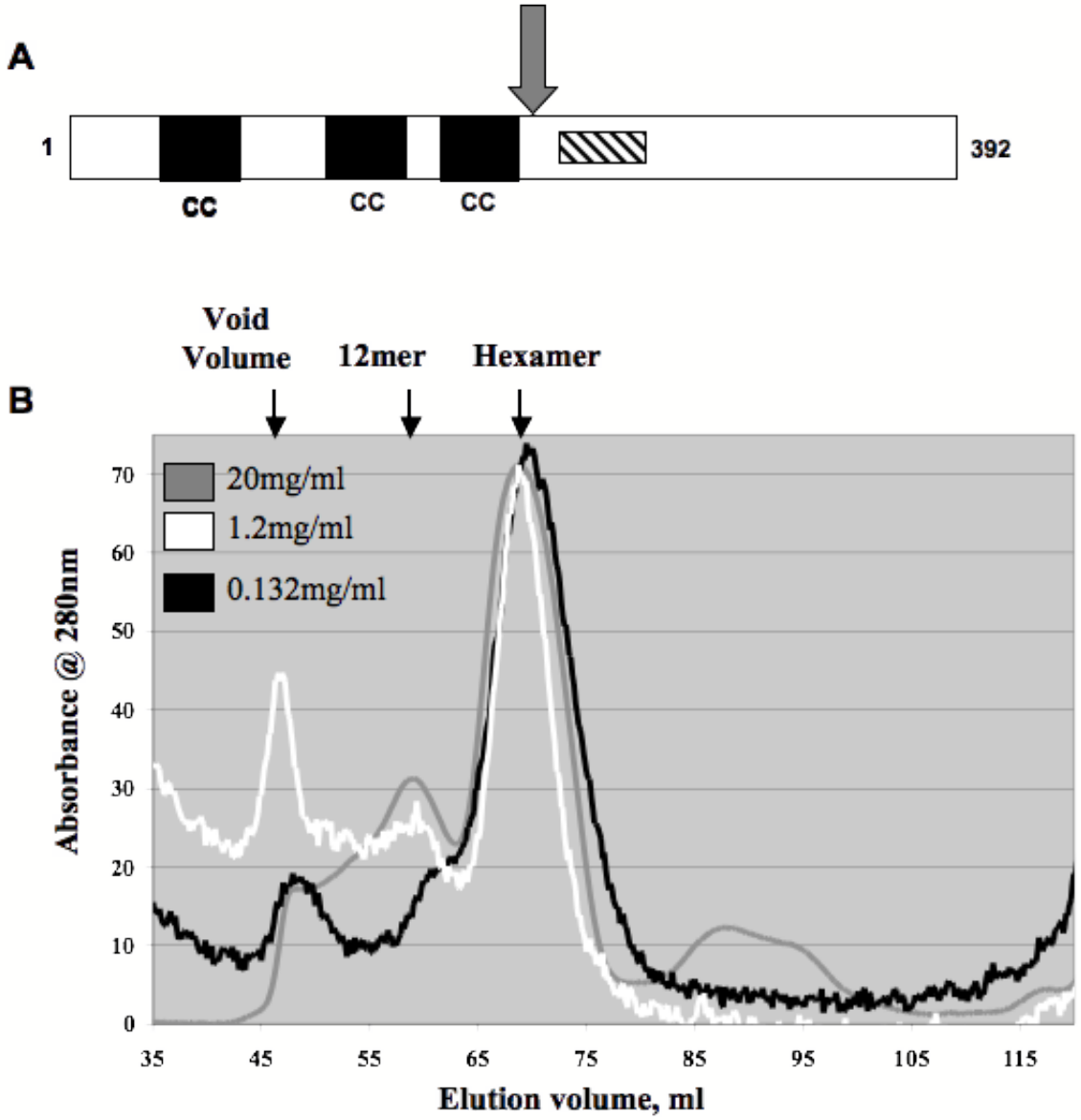

Figure 7. *NAP1CC appears stable after refolding.* **A)** Cartoon diagram of NAP1 protein domains. The gray arrow denotes where the protein was truncated, by introduction of a stop codon. CC, coiled coil **B)** Samples of NAP1CC were eluted in 20mM HEPES, pH 7.5, 0.5 M NaCl, 5% glycerol and 1 mM βME from an S200 Superdex size exclusion chromatography column. At various concentrations (20 mg/ml, gray; 1.2 mg/ml, white; 0.132 mg/ml, black), three peaks are observed. The major peak corresponds to a hexameric species, two minor peaks consist of a dodecamer and large or aggregated protein. All chromatographs were normalized to fit on a single chart. Oligomeric states of peaks were determined by comparison to gel filtration standards.

3.1.4 Analytical Ultracentrifugation (AUC) (completed by Dr. R. Ghirlando)

As a complementary technique AUC was utilized to obtain a more accurate molecular weight. The data collected via AUC includes sedimentation and diffusion coefficients that contain information concerning the size and shape of a protein. A buoyancy term is also derived, which can account for the tumbling limitations of SEC. Using all these pieces of data, a more accurate molecular weight can be calculated. In collaboration with Dr. Rodolfo Ghirlando (NIDDK, NIH), AUC sedimentation velocity studies were performed on the "hexamer" species to confirm the data collected by SEC (Figure 7). Concentrations ranging from 17 to 137mM (0.435 to 3.49mg/ml) were tested to determine oligomeric state and examine concentration dependence of association (Figure 8). AUC analysis of this protein indicates that NAP1CC actually behaves as a dimer in vitro. This validated the need to include both SEC and AUC to determine accurate homointeractions of these coiled-coil domain proteins.

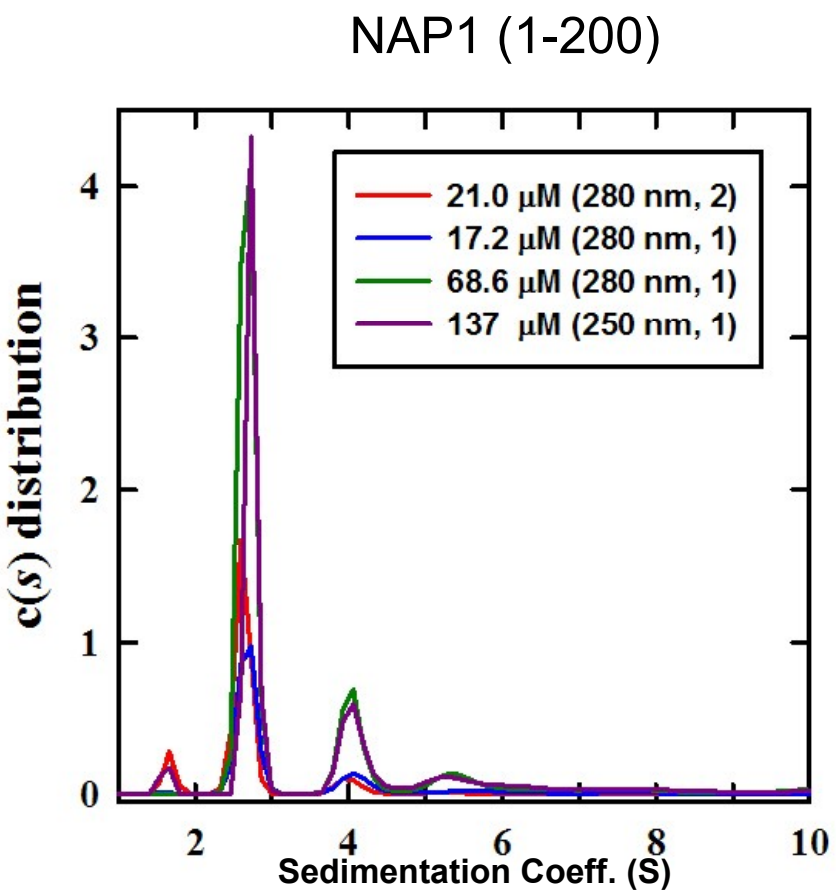

Figure 8. *NAP1CC is a dimeric species by AUC.* Analytical ultracentrifugation data, sedimentation coefficient (S) profiles, of NAP1CC were collected for samples from a concentration range of 17.2 to 137 μM in 0.02 M HEPES, pH 7.5, 0.5 M NaCl, 5% glycerol, 1 mM βME. Samples were run at 55 K rpm and 20°C. The major peak having an S value of 2.67 corresponds to a molecular weight of ~44 kDa just slightly less than a NAP1CC dimer (~51 kDa).

AUC data were collected by Dr. R. Ghirlando at NIDDK, NIH, Bethesda, MD.

3.2 Attempts to obtain full-length TBK1 and IKKε via Baculovirus system

3.2.1 Generation of TBK1/IKKε full-length Baculovirus

Dr. Katherine Fitzgerald kindly provided the pFASTBAC vector containing an N-terminal FLAG-tagged TBK1 gene (Figure 9A). This vector backbone was used to construct an equivalent expression vector with the IKKε gene using standard molecular biology techniques (Stratagene). Both TBK1 and IKKε pFASTBAC constructs were then DNA sequence confirmed. Bacmid DNA was generated using Invitrogen's Bac-to-Bac® Baculovirus protocol (Figure 9B-C). Virus was amplified in additional cultures to yield 500ml of viable virus per construct at a titer between $1x10^8$ plaque forming units/milliliter (pfU/ml) and $1x10^9$ pfU/ml.

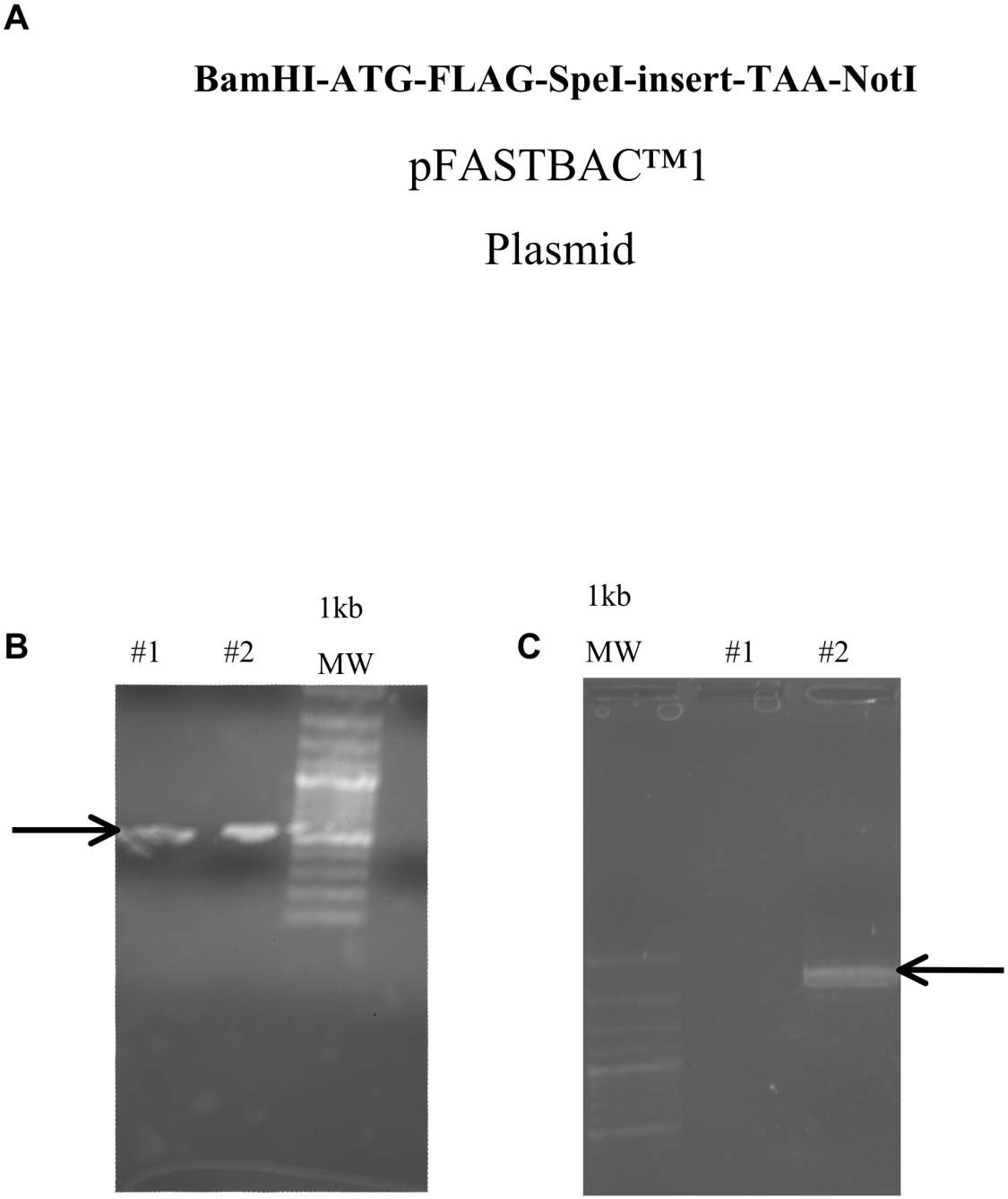

Figure 9. *Confirmation of successful ligation of TBK1/IKKε into Bacmid DNA.* **A)** Cartoon diagram of pFastBac plasmid containing either the full-length TBK1 or IKK ε gene. **B)** PCR screen using purified TBK1 FL Bacmid DNA as templates (2 in total), using an M13F primer specific for the Bacmid vector and an internal primer inside the TBK1 construct. Both were positive when screened (indicated by blue arrow). **C)** PCR screen using purified IKKε FL Bacmid DNA as templates (2 in total), using an M13F primer specific for the Bacmid vector and an internal primer inside the IKK ε construct. Only 1 sample screened was positive (indicated by black arrow).

3.2.2 Expresssion and Purification of TBK1/IKKε FLAG-tagged proteins

Sf9 cells cultured in suspension were infected with TBK1 or IKKε incorporated baculovirus as described in the literature (14) to express the kinases. The cells were infected at a cell density of 1.5-2 x 10^6 cells/ml with a multiplicity of infection (MOI) of three. Cells were harvested fourty-eight hours post-infection and then lysed by emulsification (Avestin Emulsiflex C3) at 20,000 psi. The kinases were purified from clarified cell lysates using anit-FLAG M2-agarose affinity column chromatography as per manufacturer's protocol (Sigma) and eluted using 0.34mg/ml FLAG peptide in two twenty-five milliliter fractions and concentrated by ultra-filtration (Amicon Ultra- 3000 molecular-weight cut-off (MWCO). To remove FLAG peptide from elution fractions it was purified by separation on a Superdex 200 column (Figure 10) and checked for purity by separation by SDS-PAGE, coomassie stain (Figure 11A). Fractions containing kinase were concentrated and protein concentration was determined by Biorad assay. Kinases were stored at -80 degrees Celsius in kinase storage buffer: 20mM Tris-HCl (pH 7.6), 150mM NaCl, 0.1% Nonidet P-40, 10% glycerol, 20mM NaF, 20mM β-glycerophosphate, 1mM EDTA, 5mM DTT, 1 EDTA-free protease inhibitor tablet, 0.1%BSA as detailed (14). Low protein yields, limited the use of recombinant kinase proteins in future assays.

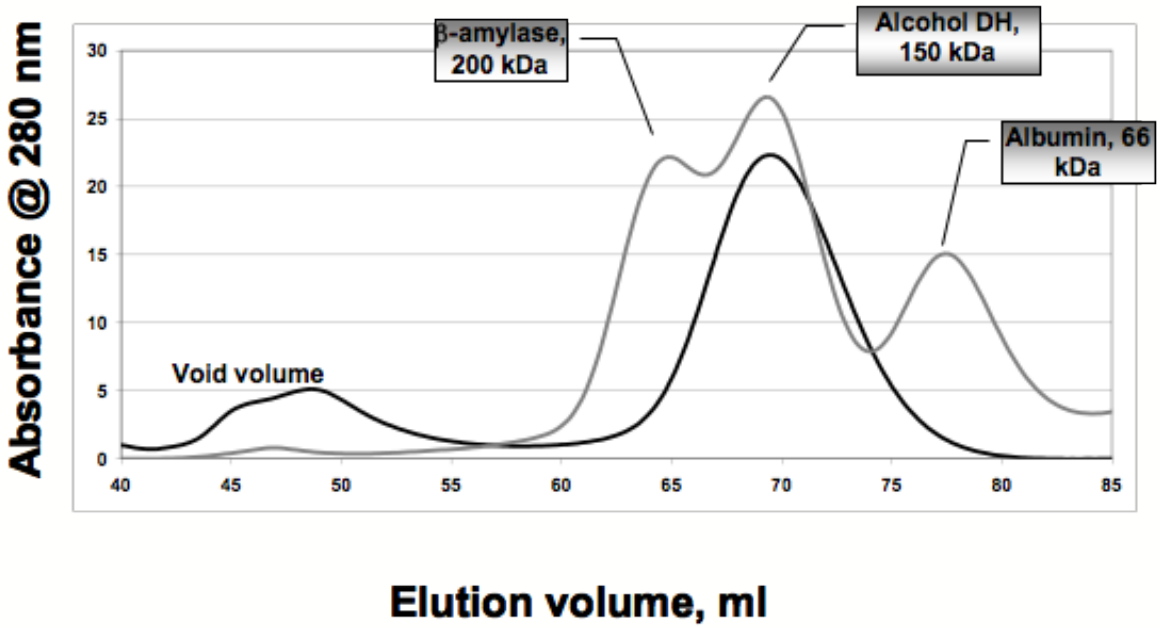

Figure 10. *SEC analysis of TBK1 FL suggests dimeric structure.* TBK1 purified from Sf9 cells was eluted in 20mM HEPES, pH 7.5, 0.5 M NaCl, 5% glycerol and 1 mM βME from an S200 Superdex size exclusion chromatography column. The TBK1 elution profile is shown in black. The major peak elutes at approximately 150kDa, which is slightly less than the weight of an ideal dimer (TBK1 MW= 87kDa). IKKε (MW= 82.21kDa) has a similar elution pattern (data not shown). Oligomeric states of peaks were determined by comparison to gel filtration standards, shown in gray and labeled accordingly.

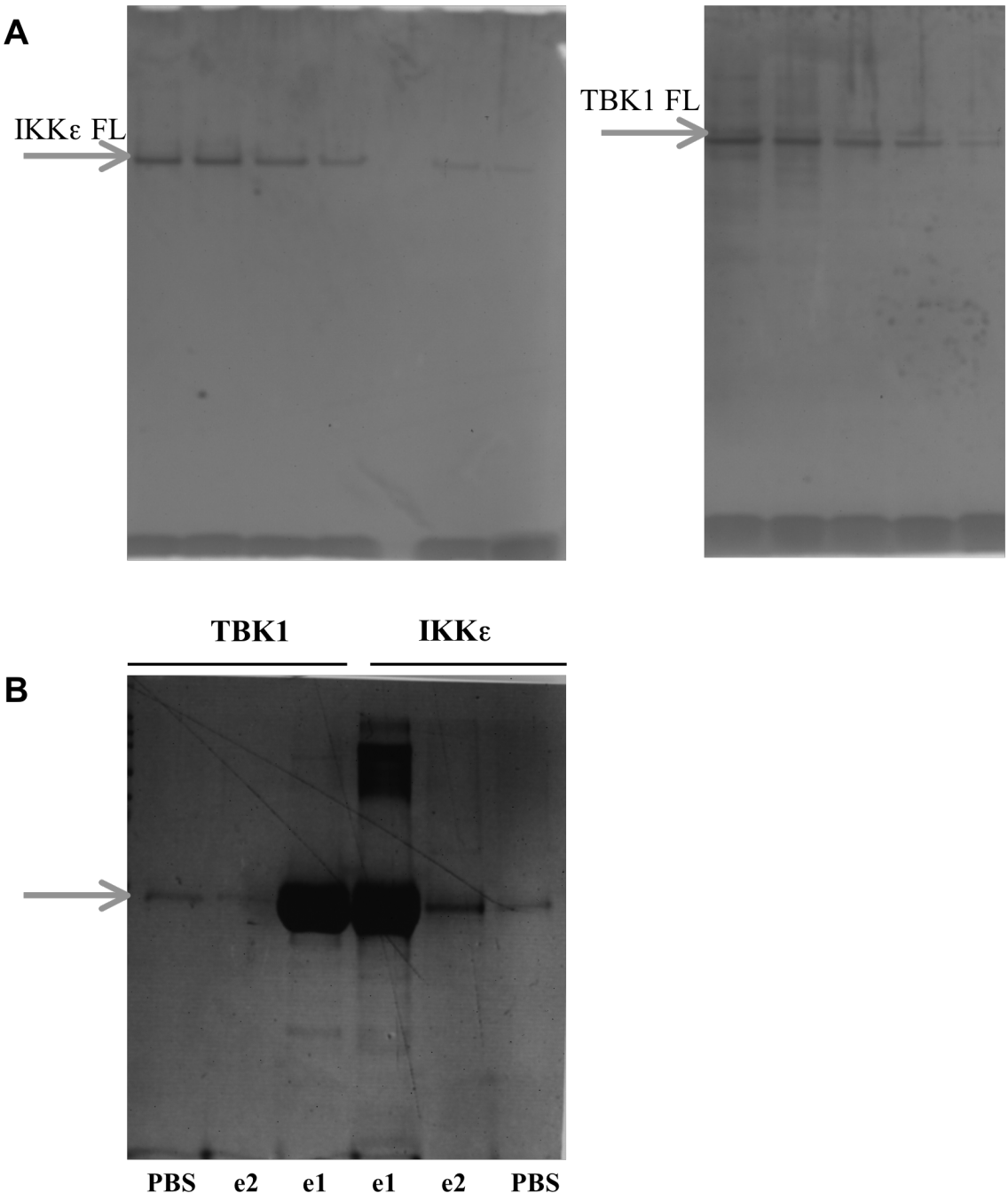

Figure 11. *Recombinant Protein Kinase Expression.* Samples were run on 10% Bis-Acryl SDS-PAGE gels showing recombinant protein expression from SEC fractions. **A)** Full-length FLAG-tagged TBK1 and IKK ε protein purified from Sf9 insect cells using FLAG-affinity resin. **B)** GST-tagged scaffold binding motif (SBM) TBK1 and IKK ε protein domain were purified using Glutathione Sepharose Transferase 4B resin. Both of the two twenty-five ml elutants and a 10ml 1X PBS Wash were analyzed for purifty. Abbreviations the same as in Figure 1. SBM, scaffold binding motif; KBD, kinase-binding domain

3.3 Nak-associated protein 1 (NAP1) interactions via kinase-binding domain (KBD) interactions

3.3.1 Generation of CFP/YFP-tagged constructs

Thus, in order to examine the potential interactions between TBK1/IKKε and the scaffold protein, NAP1, a smaller domain of the kinases, as well as, for the scaffold protein, were generated. Previous work completed in the lab lead to generation of cyan fluorescent protein (CFP) and yellow fluorescent protein (YFP) fusion proteins containing NAP1 kinase-binding domain (KBD) and TBK1 scaffold-binding motif (SBM) peptides. For example, NAP1 KBD (residues 216-255), the target gene, was inserted into the pET15b vector that included a N-terminal 6X His-tag followed downstream by a CFP molecule and then the target gene (Figure 12A), in this case NAP1 KBD (residues 216-255). A similar construct was generated using YFP that was fused with the SBM of TBK1 (residues 700-722), for Fluorescence-resonance energy transfer (FRET) pairing experiments with NAP1 KBD. CFP and Citrine proteins, containing no peptides, were also generated to serve as controls for the FRET experiments.

However, purification of these constructs showed that they all expressed as dimeric species. It was determined that a key mutation needed to be made to force the fluorophores to behave monomeric. Quikchange mutagenesis kits (Stratagene) that employed standard molecular biology and polymerase chain reaction (PCR) techniques were used, as per manufacturer's protocol, to mutate residues to make the fluorescent proteins monomeric (A206K). Furthermore, a mutation was introduced to change YFP to

Citrine (Q69M), an YFP variant, because of its emission range overlap with CFP excitation range, which is a requirement for good FRET pairing.

A

ATG-6XHis-NdeI-FP-XhoI-insert-TAA-BamHI

pET15b

B

ATG-GSTtag-BamHI-insert-TAA-XhoI

pGEX-4T™1

Figure 12. *NAP1 KBD is a dimeric species by SEC*. **A)** Cartoon diagram of monomeric cyan fluorescent protein (mCFP) NAP1 KBD plasmid. **B)** Cartoon diagram of glutathione-S-transferase (GST) tagged kinase SBM plasmid. All constructs were generated for use in fluorescence resonance energy transfer studies.

3.3.2 Generation of GST-TBK1/IKKε SBM for labeling with Alexa-Fluor 546

Both TBK1 and IKKε (687-709) SBMs were inserted into the pGEX-4T1 vector (Figure 12B), a bacterial expression vector that includes an N-terminal Glutathione-S-transferase tag for affinity chromatography purification following expression. Quikchange mutagenesis kits (Stratagene) that employed standard molecular biology and polymerase chain reaction (PCR) techniques were used, as per manufacturer's protocol, to insert a cysteine residue at the N-terminal of the TBK1 SBM peptide that allows for linkage with an Alexa-Fluor 546 molecule and use in small-molecule FRET experiments.

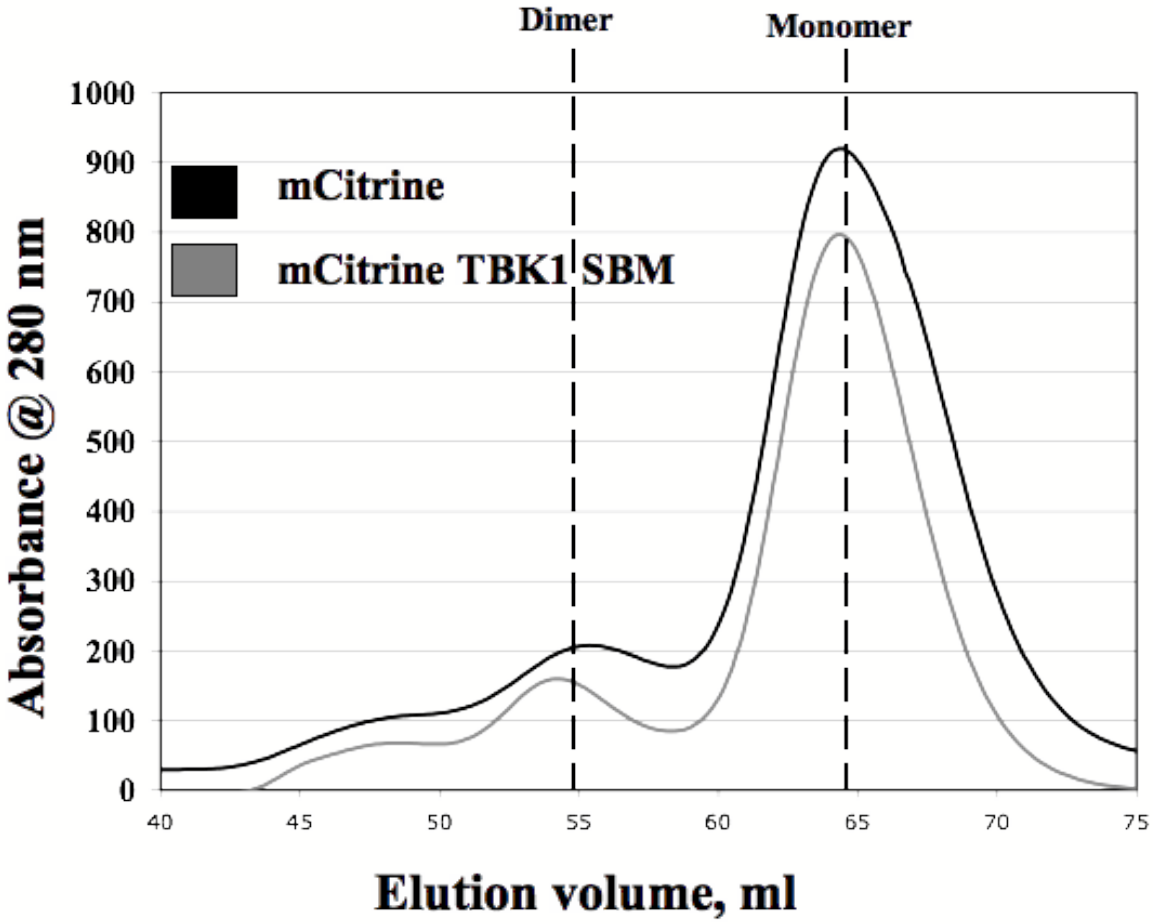

Figure 13. *TBK1 SBM elutes monomeric via SEC.* Monomeric citrine fluorescent protein (mCitFP) and monomeric Citrine TBK1 SBM (700-722) fluorescent protein (mCitFP TBK1 SBM) fusion proteins were separated on an S200 Tricorn Superdex size exclusion chromatography column. mCitFP, shown in black, and mCitFP TBK1 SBM, shown in gray, both eluted as a monomeric species. Elution volume of a dimeric species and monomeric species are denoted. Oligomeric states were determined by comparison of elution patterns to globular, well-characterized gel filtration standards.

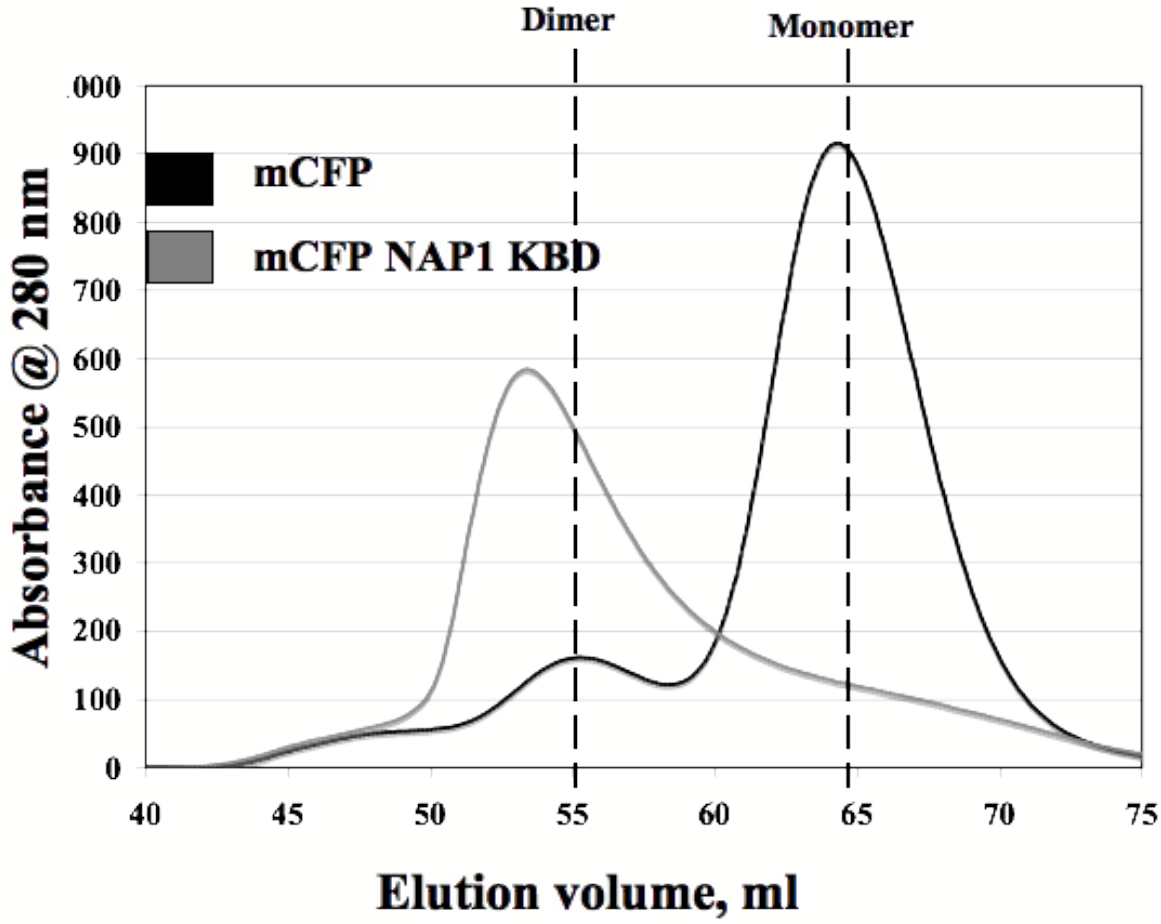

Figure 14. *NAP1 KBD mediates dimer formation via SEC.* Monomeric cyan fluorescent protein (mCFP) and monomeric cyan NAP1 KBD (216-255) fluorescent protein (mCFP NAP1 KBD) fusion proteins were separated on an S200 Tricorn Superdex size exclusion chromatography column. mCFP, shown in black, eluted as a monomeric species and mCFP NAP1 KBD, shown in gray, eluted as a dimeric species. Oligomeric states were determined by comparison of elution patterns to globular, well-characterized gel filtration standards.

3.3.3 Expression and Purification

The pET15b constructs are purified from cell lysates by binding to a Ni^{2+} charge immobilized metal affinity chromatography (IMAC) resin, HISTRAP, washed with binding buffer **(**20 mM $NaPO_4$ (pH 8), 0.5M NaCl, 1mM βME**)** and eluted using a gradient of imidizaole (0 – 0.5M) in binding buffer as modified per manufacturer's instructions (GE Healthcare). Fractions containing target protein, as assessed by separation on SDS-PAGE and coomassie staining, were pooled, concentrated and further purified by separation on a Superdex 200 column (Figure 13-14) and checked for purity by separation by SDS-PAGE, coomassie staining (Figure 15A-B, 16A-B).

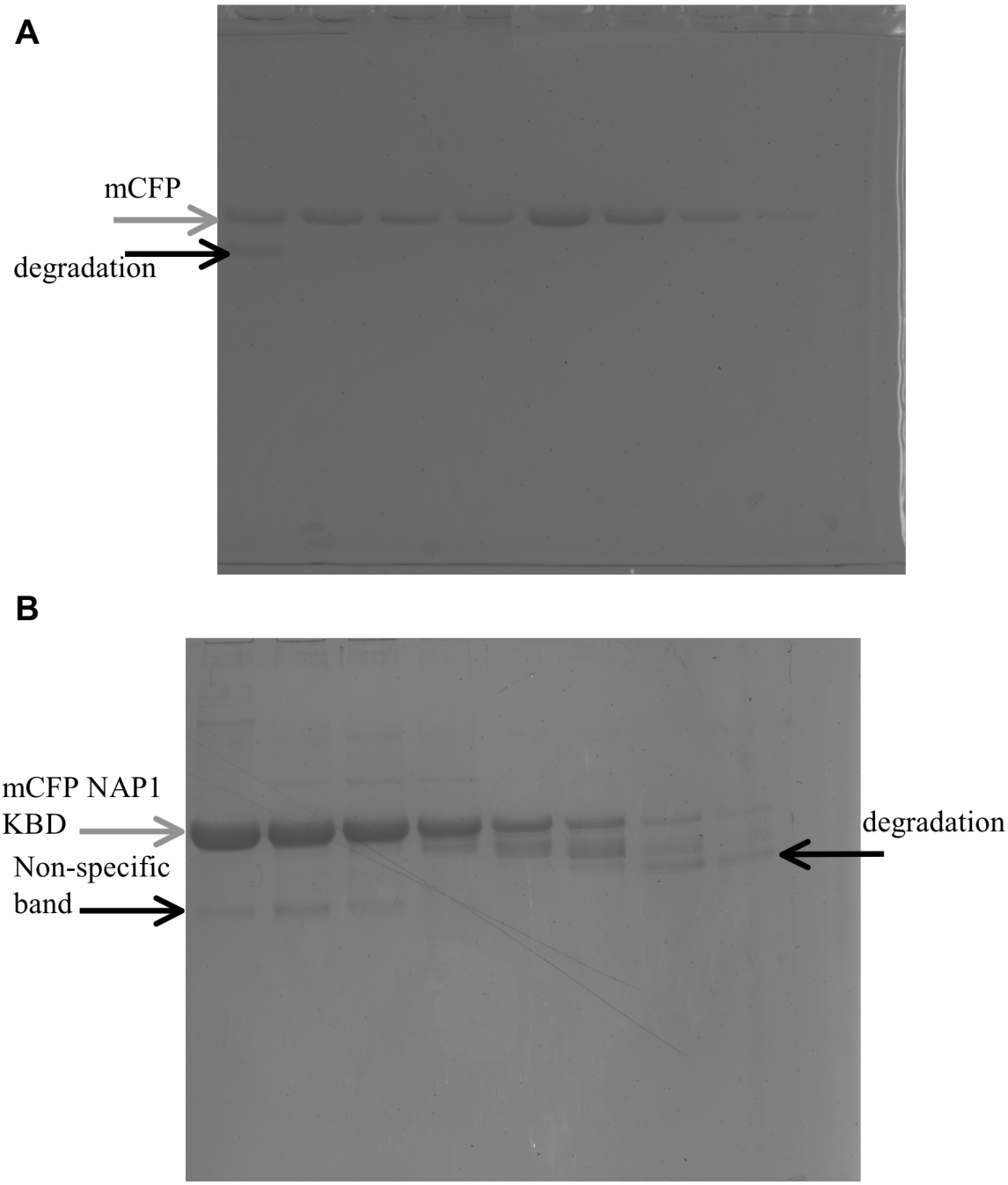

Figure 15. *Recombinant mCFP Protein Kinase Purification.* Samples were run on 10% Bis-Acryl SDS-PAGE gels showing recombinant protein expression from SEC fractions. **A)** monomeric cyan fluorescent protein (mCFP) and **B)** mCFP NAP1 KBD purification His-tagged proteins purified using Ni-NTA resin. Gray arrows indicate full-length protein expression and black arrows denote degradation of product and non-specific bands. Any fractions containing degradation are not pool and used for future experiments. Abbreviations the same as in Figure 1. SBM, scaffold binding motif; KBD, kinase-binding domain; CC, coiled-coil.

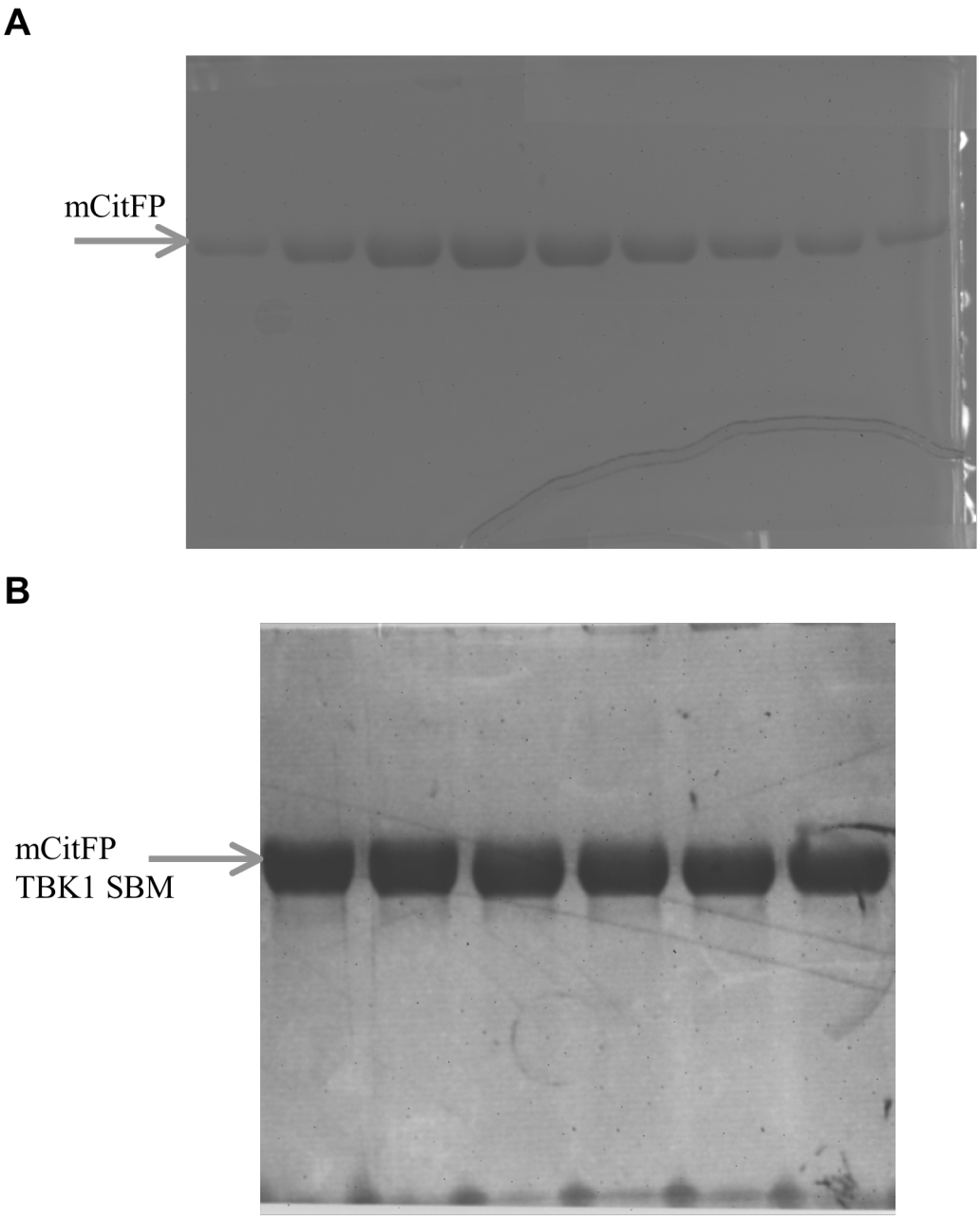

Figure 16. *Recombinant mCitFP Protein Kinase Purification.* Samples were run on 10% Bis-Acryl SDS-PAGE gels showing recombinant protein expression from SEC fractions. **A)** monomeric citrine fluorescent protein (mCitFP) and **B)** mCitFP TBK1 SBM purification His-tagged proteins purified using Ni-NTA resin. Gray arrows indicate full-length protein expression. Abbreviations the same as in Figure 1. SBM, scaffold binding motif; KBD, kinase-binding domain; CC, coiled-coil.

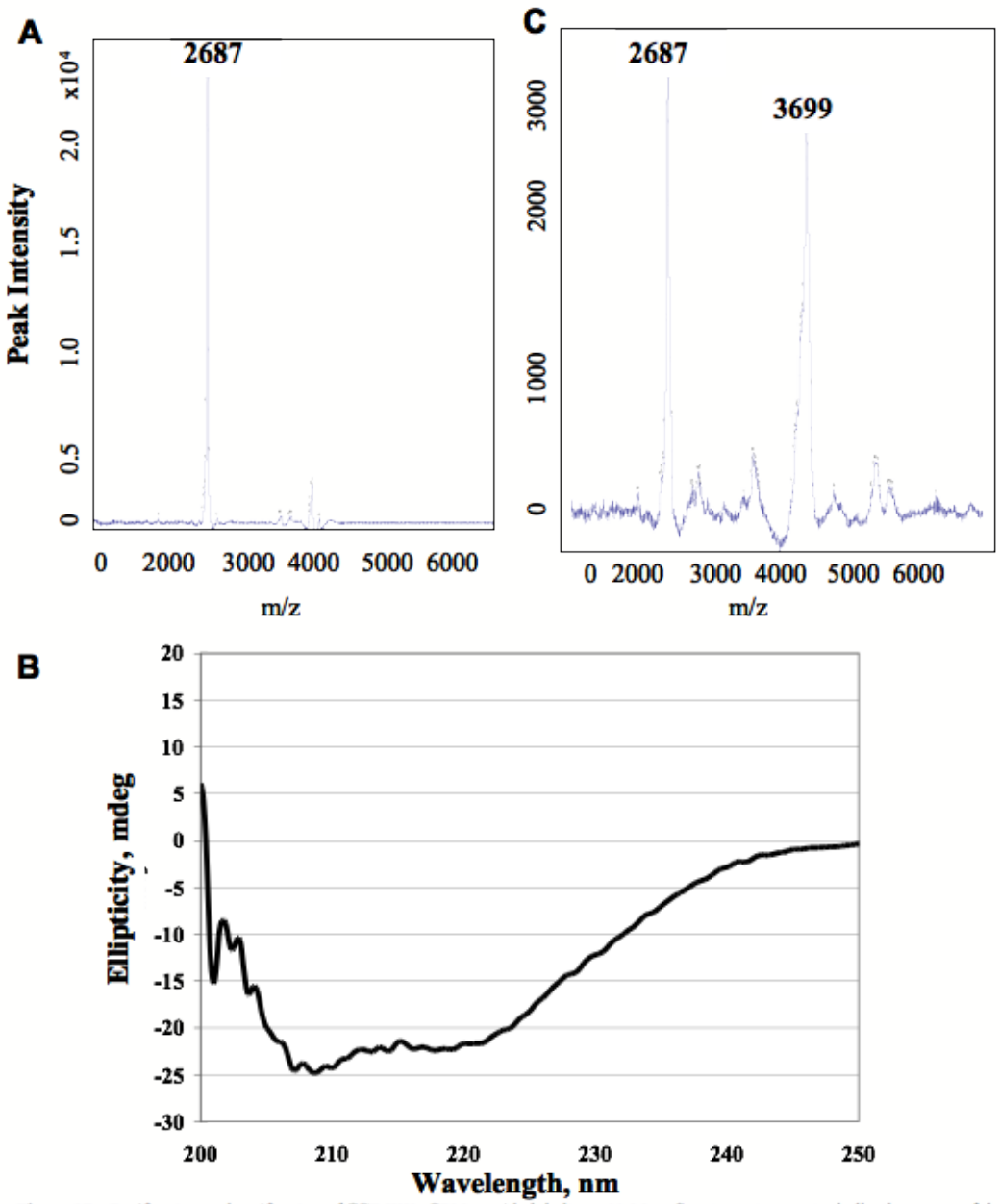

Figure 17. *Purification and verification of GST-IKKε SBM peptide labeling.* **A)** Mass Spectrometry spectra indicating successful cleavage and purification of IKKε SBM peptide. **B)** CD Spectra of IKKε SBM peptide (in 20mM HEPES pH 7.5, 150mM NaCl, 1mM βME) from 200-250nm shows negative ellipticity at 208 and 222 nm consistent for alpha helical content.. **C)** Mass Spectrometry spectra indicating successful labeling of IKKε SBM peptide with AF546.

Mass Spectrometry data collected by James Marion

The GST fusion proteins, using the pGEX-4T1 vector, were expressed in bacteria as a soluble protein and purified from clarified cell lysates using standard protocol provided by the manufacturer (GE Healthcare) for Glutathione Sepharose 4B resin and assessed for purity by separation by SDS-PAGE and coomassie stain (Figure 11B). Following successful purification of the GST IKKε SBM protein, the GST-tag was cleaved with thrombin (10units/mg of target protein) per manufacturer's protocol (GE Healthcare) and confirmed via mass spectrometry (Figure 17A). Pure peptide was assessed for secondary structure formation via CD spectrum (Figure 17B) and appears to have mainly alpha helical content.

3.3.4 NAP1 KBD homo-interactions analyzed via SEC

The kinase binding domain (KBD) of NAP1 was also examined for homo-interactions using SEC. During initial purification experiments it eluted as a dimer, while the other CFP/Citrine-tagged proteins eluted as a monomer (Figure 13-14). To determine if the dimer is concentration dependent, mCFP NAP1 KBD was run over a S200 tricorn column (GE) in the following buffer: 20 mM HEPES (pH 7.5), 150mM NaCl, and 1mM βME. mCFP NAP1 KBD was analyzed over the concentration range 1 to 6mg/ml (Figure 18). The results showed that, at concentrations below 2mg/ml, mCFP NAP1 KBD eluted as a monomer, while at concentrations above this threshold it eluted as a dimeric species. Furthermore, when mCFP, with no peptide fused, was analyzed at the 6mg/ml

concentration it eluted as a monomeric species. Thus, the NAP1 KBD is mediating the dimer formation and not the CFP molecule.

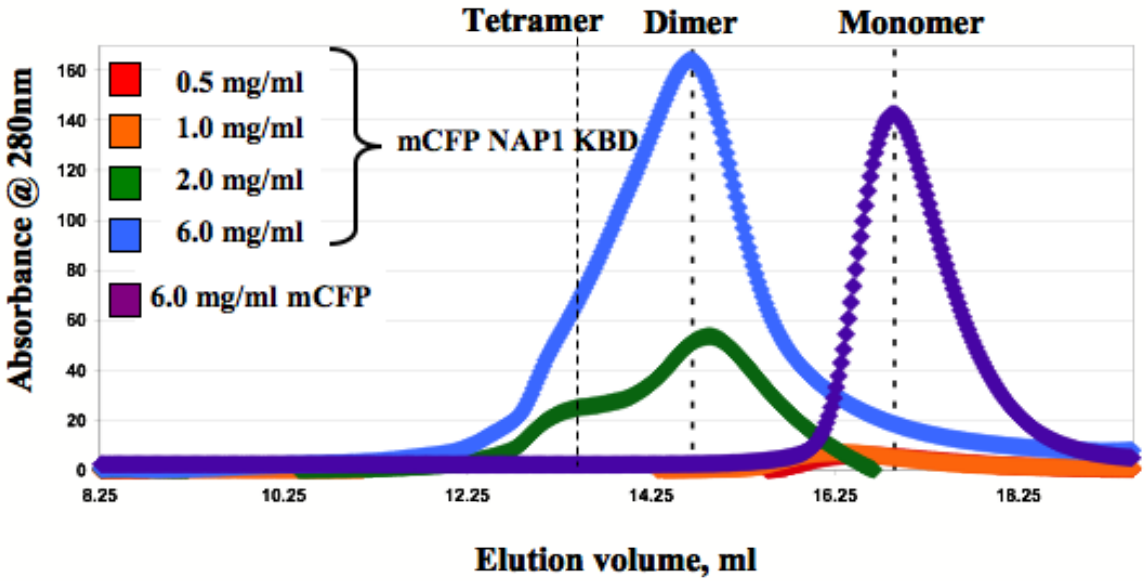

Figure 18. *mCFP NAP1 KBD forms a concentration dependent dimer.* Monomeric cyan fluorescent protein (mCFP) NAP1 KBD fusion protein was separated on an S200 Tricorn Superdex size exclusion chromatography column. At 0.5 mg/ml mCFP NAP1 KBD elutes as a monomer. The 1 mg/ml elution peak is shifted slightly but remains monomeric. At 2 and 6mg/ml two species were observed, a dominant dimer species and a tetramer species (leading shoulder). The mCFP protein at 6 mg/ml elutes as a monomer suggesting that the oligomerization observed is mediated by the NAP1 KBD peptide. Oligomeric states were determined by comparison of elution patterns to globular, well-characterized gel filtration standards.

3.3.5 NAP1 KBD homo-interactions assessed via a molecular model

It has been shown that the first 200 residues of the NAP1 protein (Figure 8) and the NAP1 KBD (Figure 18) are dimeric in structure. Other data collected in the lab (data not shown) has successfully expressed and purified GST-tagged NAP1 KBD (performed by James Marion). CD was completed to assess the secondary structure of this region of NAP1, which was determined to be almost exclusively alpha helical (data not shown). Therefore, when the two adjacent domains were combined in either the head-to-head or head-to-tail orientation, it becomes clear that, in order for both domains to have homo-interactions, the NAP1 protein must be in a head-to-head confirmation (Figure 19).

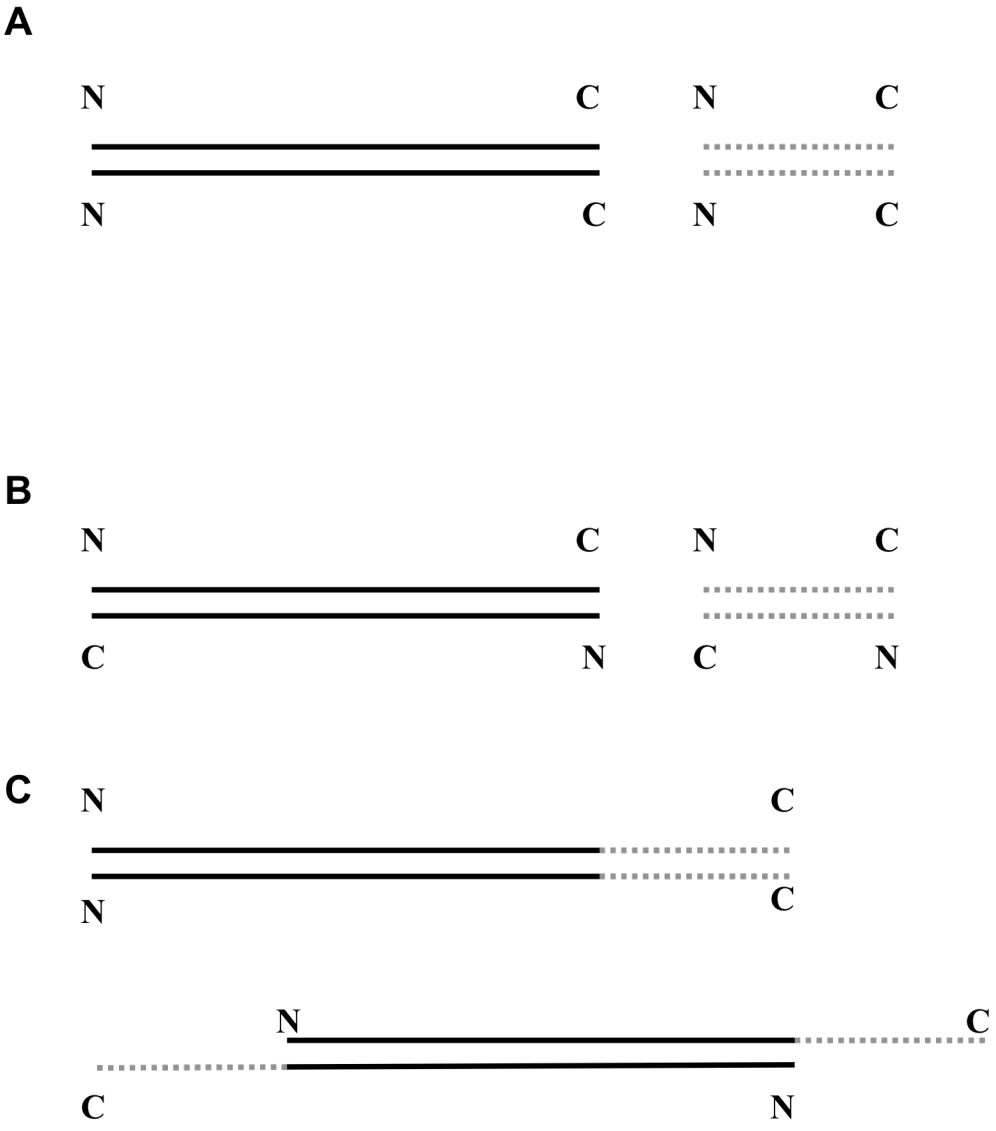

Figure 19. *NAP1 forms head-to-head dimers.* The following diagram depicts the homo-interactions of NAP1 protein domains. **A)** Shows the possible confirmations of the dimeric NAP1CC (1-200), shown in black, and NAP1 KBD (216-255), shown in gray, as head-to-head dimer and **B)** shows the same dimeric cartoon structures but in head-to-tail dimer. **C)** When the two domains are combined in either the head-to-head or head-to-tail confirmations in order for both domains to have homo-interactions the domains must be in a head-to-head confirmation.

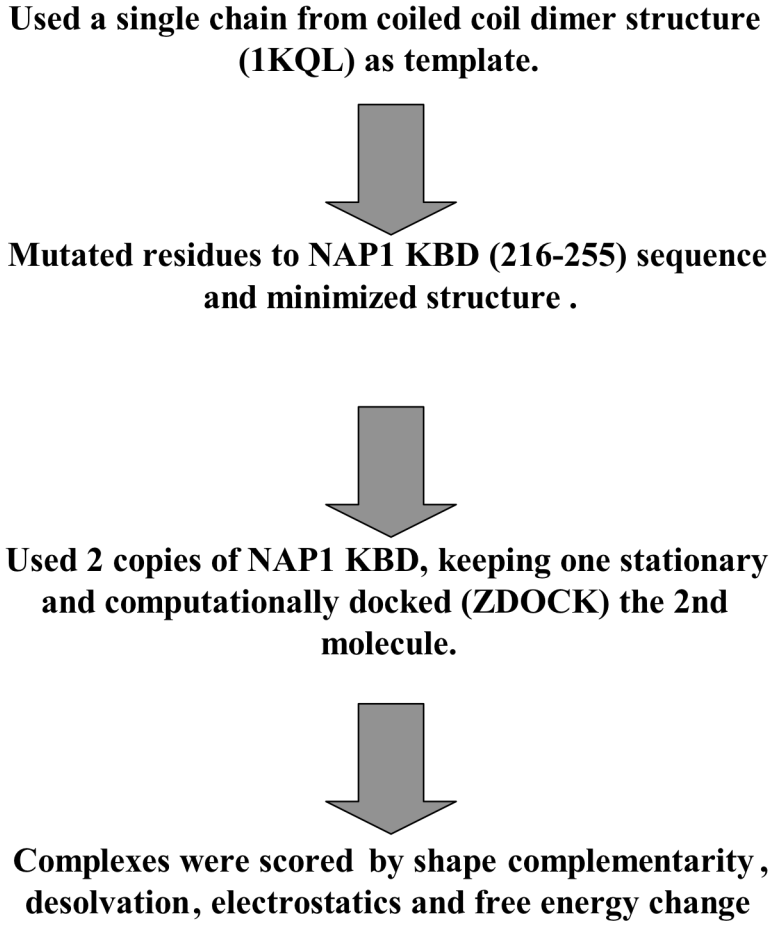

Figure 20. *Use of ZDOCK to model NAP1 KBD dimer interface.* **A)** Flowchart of NAP1 KBD model (residues 216-255) being built by mutating striated muscle alpha-tropomyosin and the GCN4 leucine zipper fusion structure (1KQL[3]) as template and then energy minimized (Phenix[4]). Computational docking (ZDOCK[5]) was used to predict dimer interface of NAP1 KBD . Complexes were scored.

To identify the essential residues for maintaining the homo-dimer of NAP1 KBD a molecular model was built; following the diagram in Figure 20. A single chain from the striated muscle alpha-tropomyosin (1KQL) was used as template; its amino acids were mutated to the NAP1 KBD (216-255) sequence using Pymol and energy minimized via Phenix (Figure 21A). Identical copies of the NAP1 KBD sequence were input into ZDOCK. Keeping one molecule stationary, the other was computationally docked to the stationary molecule.

The program scored complexes based upon shape complementarity, desolvation, electrostatics and free energy change. Additionally, based on analysis of previously collected data, (Figure 19) head-to-head complexes in the top ten scored were examined. Of the ten highest scores, only two were in the head-to-head confirmation. The two highest scoring models that met this criteria are shown in, Figure 21B-C. Both were analyzed, using Pymol, for residues that would form strong interactions at the interface of the hydrophobic core, as well as, possible electrostatic interactions; hallmarks of coiled-coil domain structures, such as NAP1 KBD.

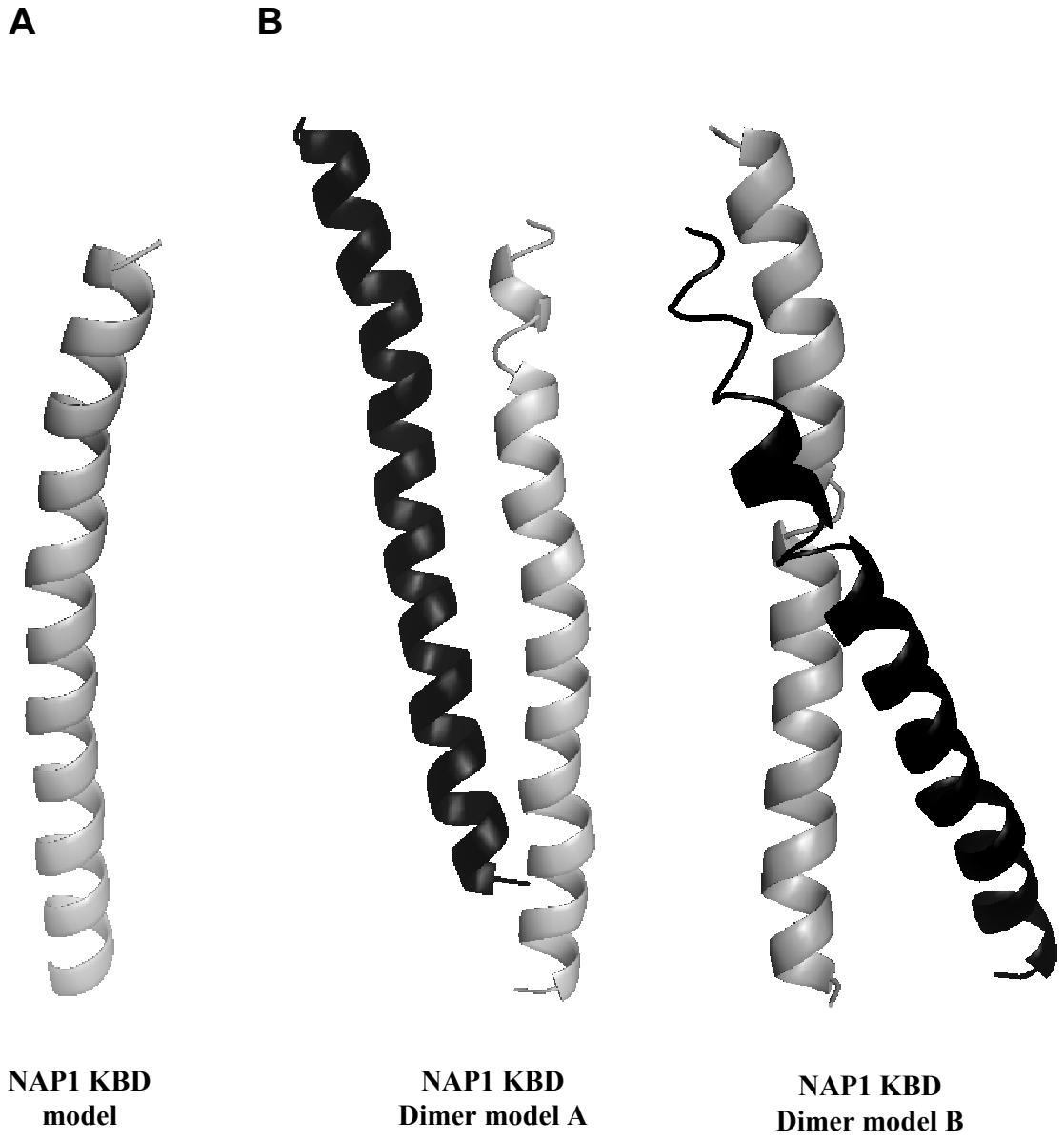

Figure 21. *Molecular model of NAP1 KBD and dimer interface.* **A)** NAP1 KBD model (residues 216-255) was built using striated muscle alpha-tropomyosin and the GCN4 leucine zipper fusion structure (1KQL[3]) as template and then energy minimized (Phenix[4]). **B)** Computational docking (ZDOCK[5]) was used to predict dimer interface of NAP1 KBD. From previous data, the dimer must form a head-to-head interaction. The two highest scoring models that met this criteria are shown.

3.4 Kinase-binding domain and Kinase Interactions

3.4.1 NAP1 KBD-TBK1 SBM Interactions

Successful purification of mCFP NAP1 KBD and mCitrine TBK1 SBM proteins allowed for assessment of hetero-interactions, as well as, any kinase protein affinity to NAP1, via FRET based assays.

Fluorescent properties of donor and acceptor

Fluorescence resonance energy transfer (FRET) is based on a couple properties. In order to achieve FRET a couple properties must be met. First, the FRET pair, donor and acceptor, must be in close contact, approximately 10-100 Angstroms. The FRET pair must be in close contact to allow for energy transfer from the donor to the acceptor. In order to achieve such a phenomenon, known as the spectral overlap, the emission spectrum of the donor must overlap with the excitation spectrum of the acceptor. To determine where this occurs for this particular FRET pair, the donor, mCFP NAP1 KBD or mCFP, was emitted at 475nm and an excitation scan (from 300-450nm) and an emission scan (from 450-650nm), exciting at 430nm, were collected separately for both mCFP NAP1 KBD and mCFP (Figure 22). The acceptor, mCitrine TBK1 SBM or mCitrine, was emitted @ 530nm and an excitation scan (from 300-525nm), and an emission scan (525-650nm), exciting at @475nm, were collected (Figure 23), as well.

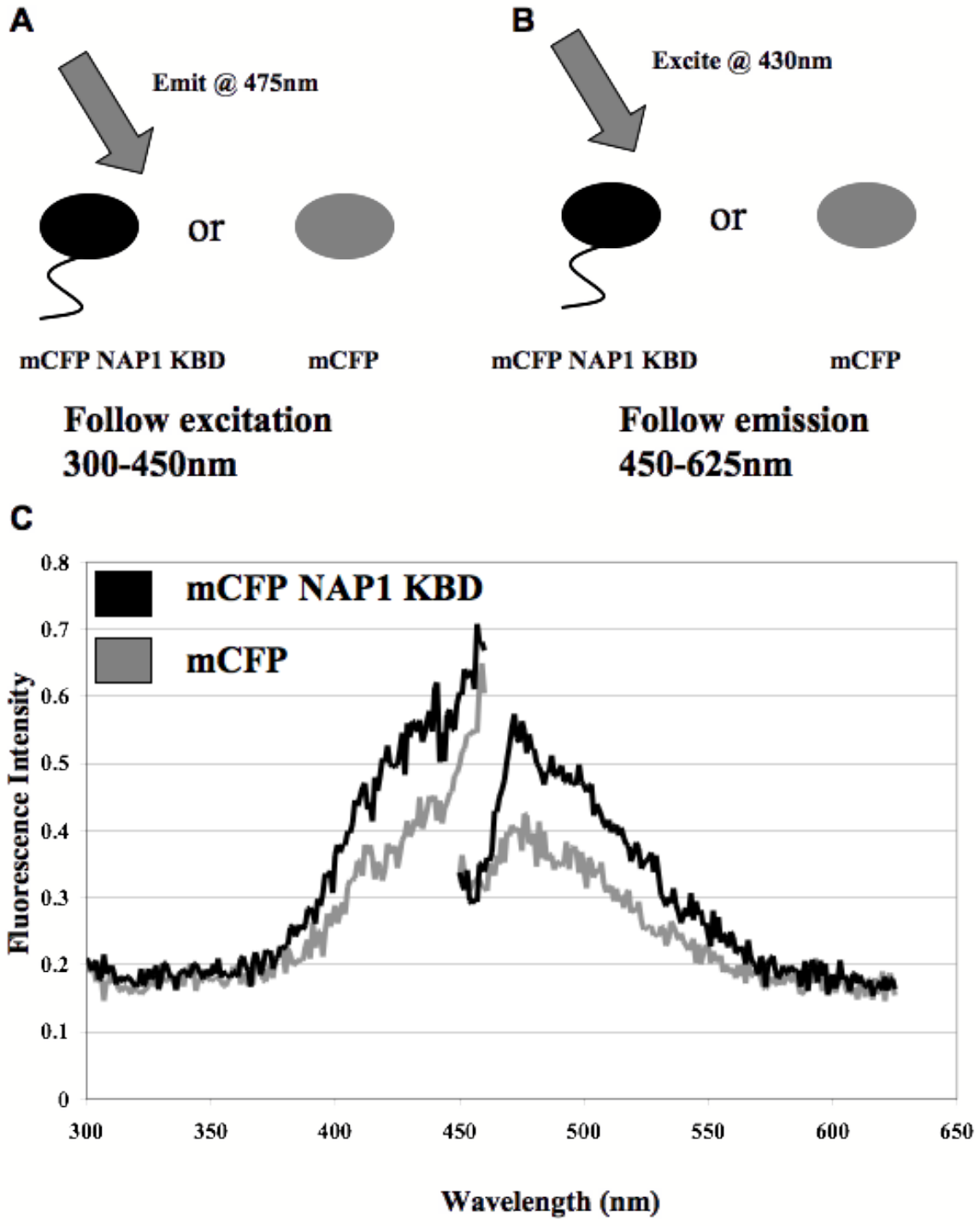

Figure 22. *Experimental design of FRET experiment* Cartoon diagram of **A)** excitation and **B)** emission scans collected for mCFP and mCFP NAP1 KBD (216-255) proteins. **C)** Graph showing the experimental excitation and emission spectrum for mCFP NAP1 KBD and mCFP with wavelength (nm) on the x-axis and fluorescence intensity on the y-axis.

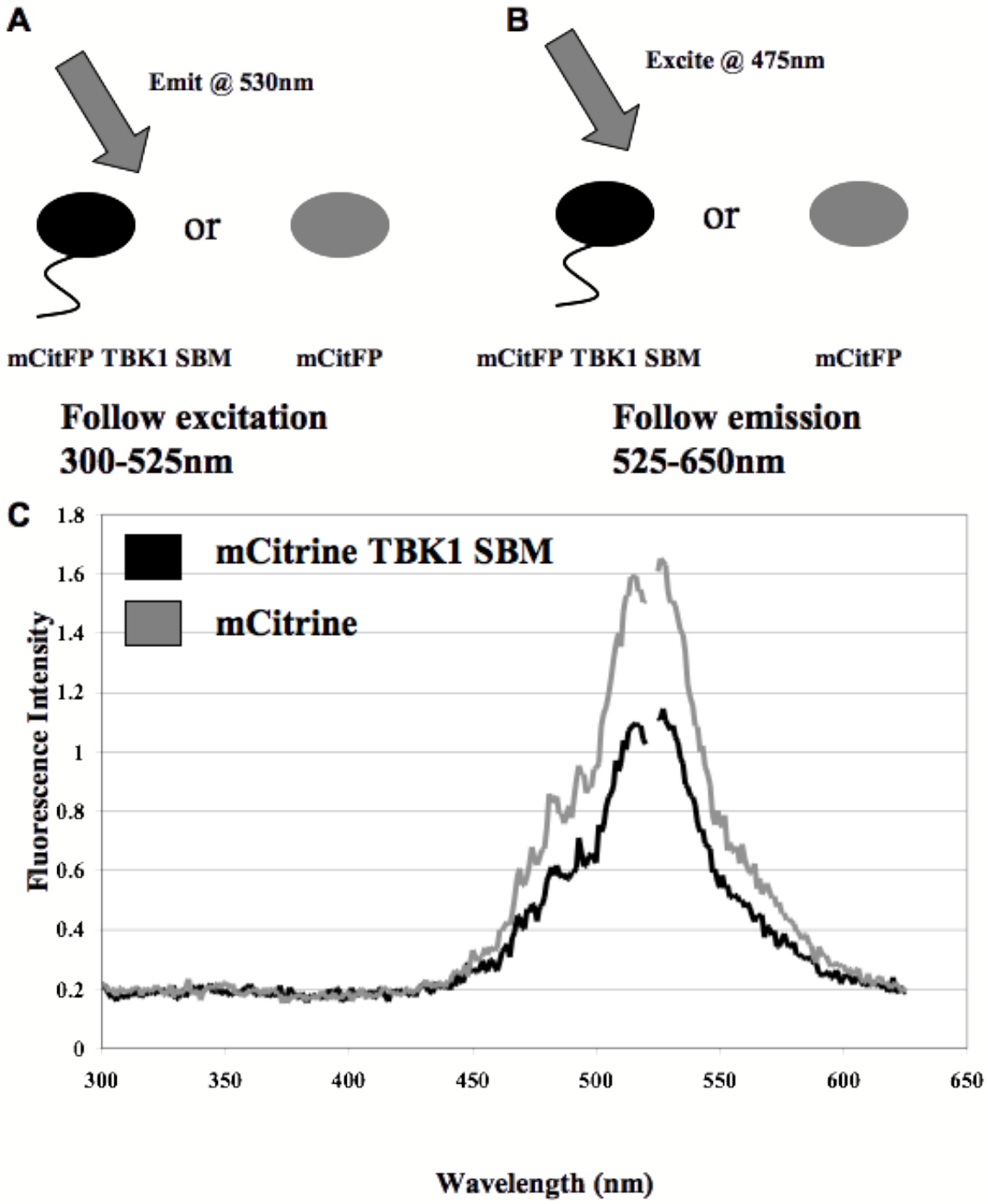

Figure 23. *Experimental design of FRET experiment.* Cartoon diagram of **A)** excitation and **B)** emission scans collected for mCitFP and mCitFP TBK1 SBM (700-722) proteins. **C)** Graph showing the experimental excitation and emission spectrum for mCitFP and mCitFP TBK1 SBM (700-722) proteins. with wavelength (nm) on the x-axis and fluorescence intensity on the y-axis.

FRET experimental set-up

Based on these spectra, the donor, mCFP NAP1 KBD, was excited at 430nm and emission spectra were collected (from 450nm to 600nm) to observe the interaction between mCFP NAP1 KBD and mCitrine TBK1 SBM (Figure 24), to obtain optimal experimental results. A total of four scans were completed every 1nm for each concentration of the acceptor. The concentration of the donor, mCFP NAP1 KBD, was held constant at 0.5μM, a concentration low enough not to force dimerization of the mCFP molecule, and aliquot into a set of cuvettes. While the acceptor, mCitrine TBK1 SBM was added to these cuvettes separately at concentrations ranging from 0-6 μM, large enough to observe FRET pairing. FRET buffer (20mM HEPES pH 7.5, 150mM NaCl, 1mM βME) was added to maintain constant volume in all cuvettes.

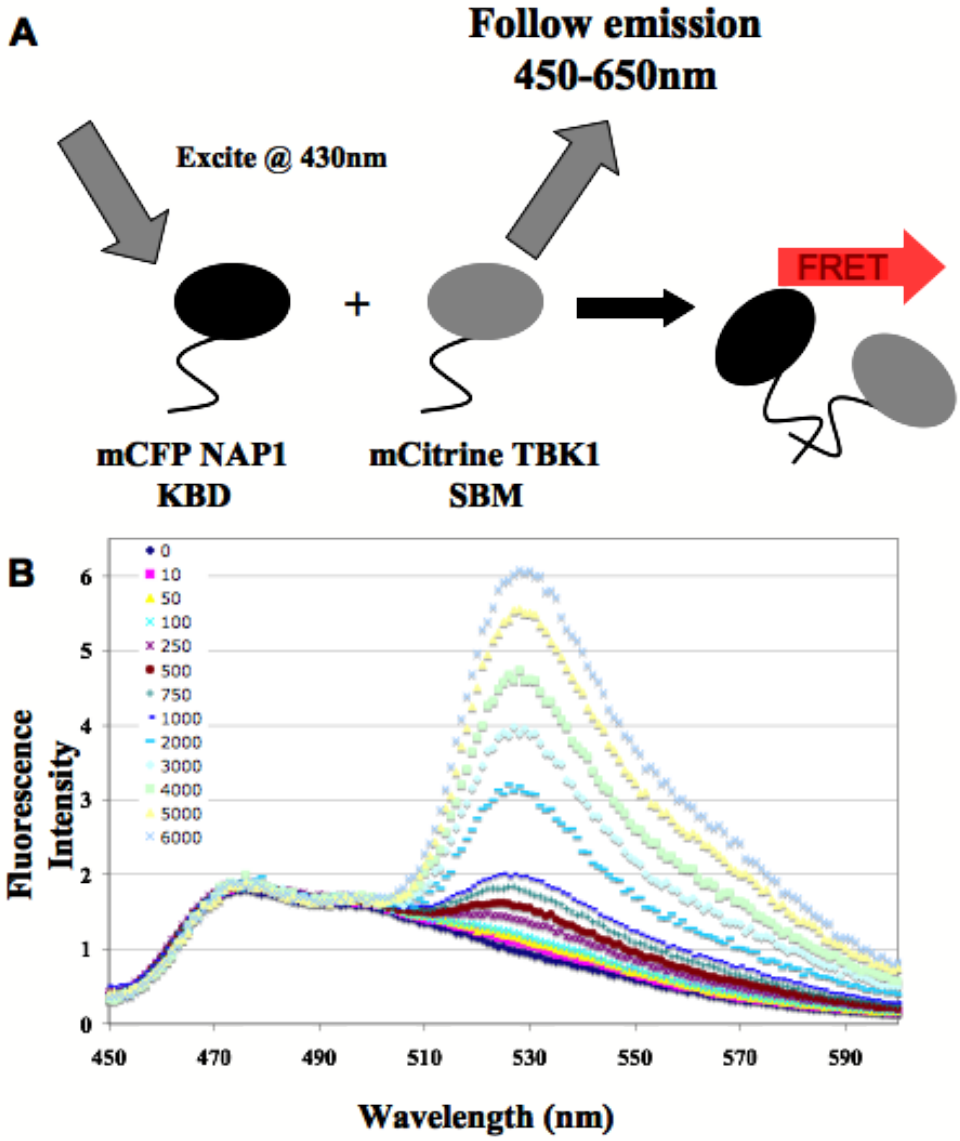

Figure 24. *FRET analysis of mCFP NAP1 KBD and mCitFP TBK1 SBM* **A)** Cartoon diagram illustrating the experimental emission spectrum for mCFP NAP1 KBD (black) and mCitFP TBK1 SBM (gray) and the range for following the emission (**B)** Graph showing the emission spectra (exciting @ 430nm) from 'mCFP NAP1 KBD + mCitFP TBK1 SBM' and following emission from 450-600nm, with the concentration of mCFP NAP1 KBD held at 0.5μM and mCitFP TBK1 SBM increased from 0-6μM with wavelength (nm) on the x-axis and fluorescence intensity on the y-axis.

While the majority of the energy transfer from donor to acceptor is from the two peptides interacting, it is possible to get non-specific interactions between the two fluorphores, mCFP and mCitrine. To correct for this, the interaction between mCFP NAP1 KBD and mCitrine (Figure 25) was observed by excitation of the donor, mCFP NAP1 KBD, at 430nm and emission spectra were colleted (from 450nm to 600nm) to measure the non-specific interaction. The experimental set-up was the same as described above.

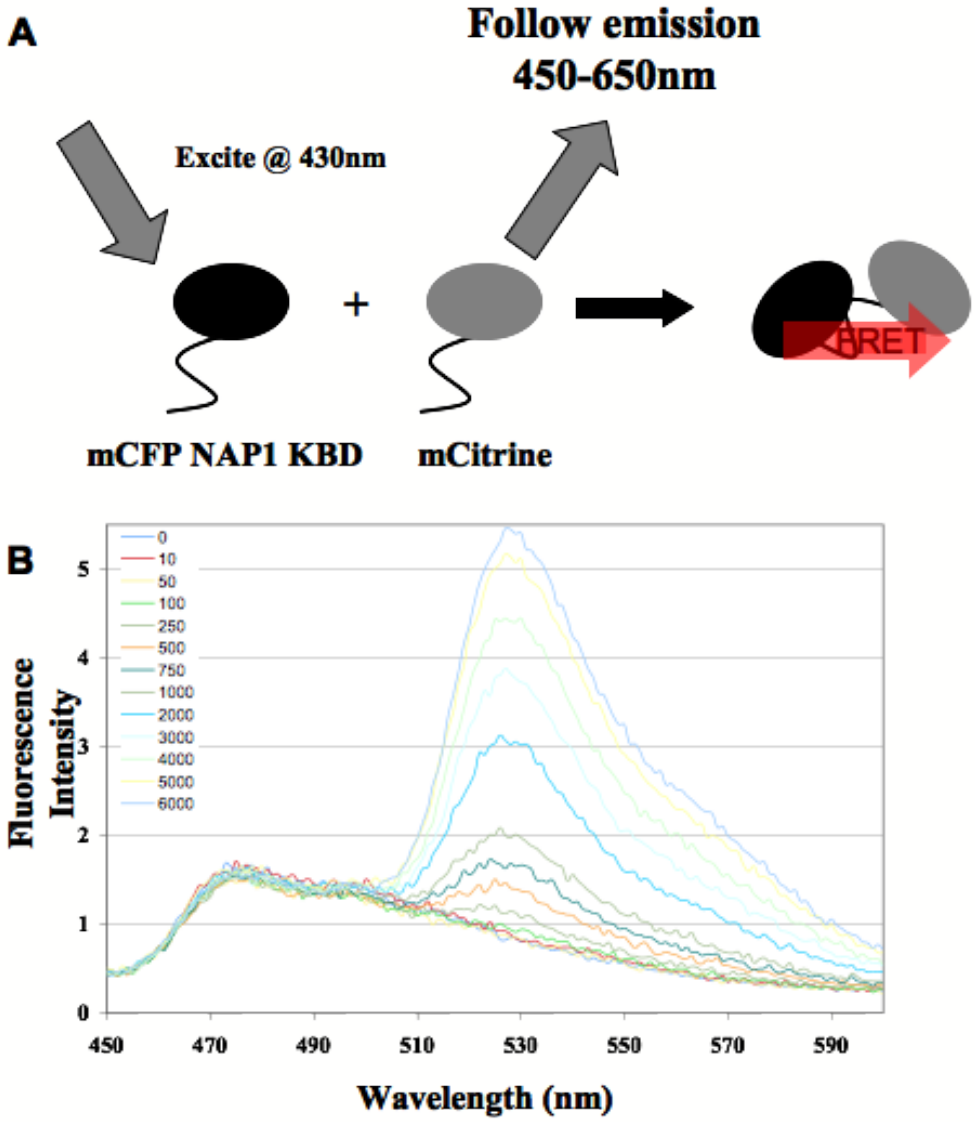

Figure 25. *FRET analysis of mCFP NAP1 KBD and mCitFP* **A)** Cartoon diagram illustrating the control emission spectrum for mCFP NAP1 KBD (black) and mCitFP (gray) and the range for following the emission (**B)** Graph showing the control emission spectra (exciting @ 430nm) from 'mCFP NAP1 KBD + mCitFP' and following emission from 450-600nm, with the concentration of mCFP NAP1 KBD held at 0.5μM and mCitFP increased from 0-6μM with wavelength (nm) on the x-axis and fluorescence intensity on the y-axis.

Data Analysis

Upon completion of the spectra, a correction factor is calculated, to adjust for difference in fluorescence intensity between the mCFP and mCitrine fluorphores. This correction factor is the fluorescence intensity between mCitrine:mCitrine TBK1 SBM at 530nm, the excitation maximum for mCitrine:

$$\frac{\text{Fluorescence Intensity @ 530nm of mCitFP}}{\text{Fluorescence Intensity @ 530nm of mCitFP TBK1 SBM}}$$

With this correction factor, (value of 1.4) any difference in fluorescence intensity between the mCFP and mCitrine fluorophores:

(experimental FI @530nm)- ((control FI @530nm)/1.4)

After this correction is applied the net fluorescence (Figure 26A) was fit to a binding curve (FI @ 530 vs. log [mCitFP TBK1 SBM (nM)] where the K_D is approximately 2μM (Figure 26B).

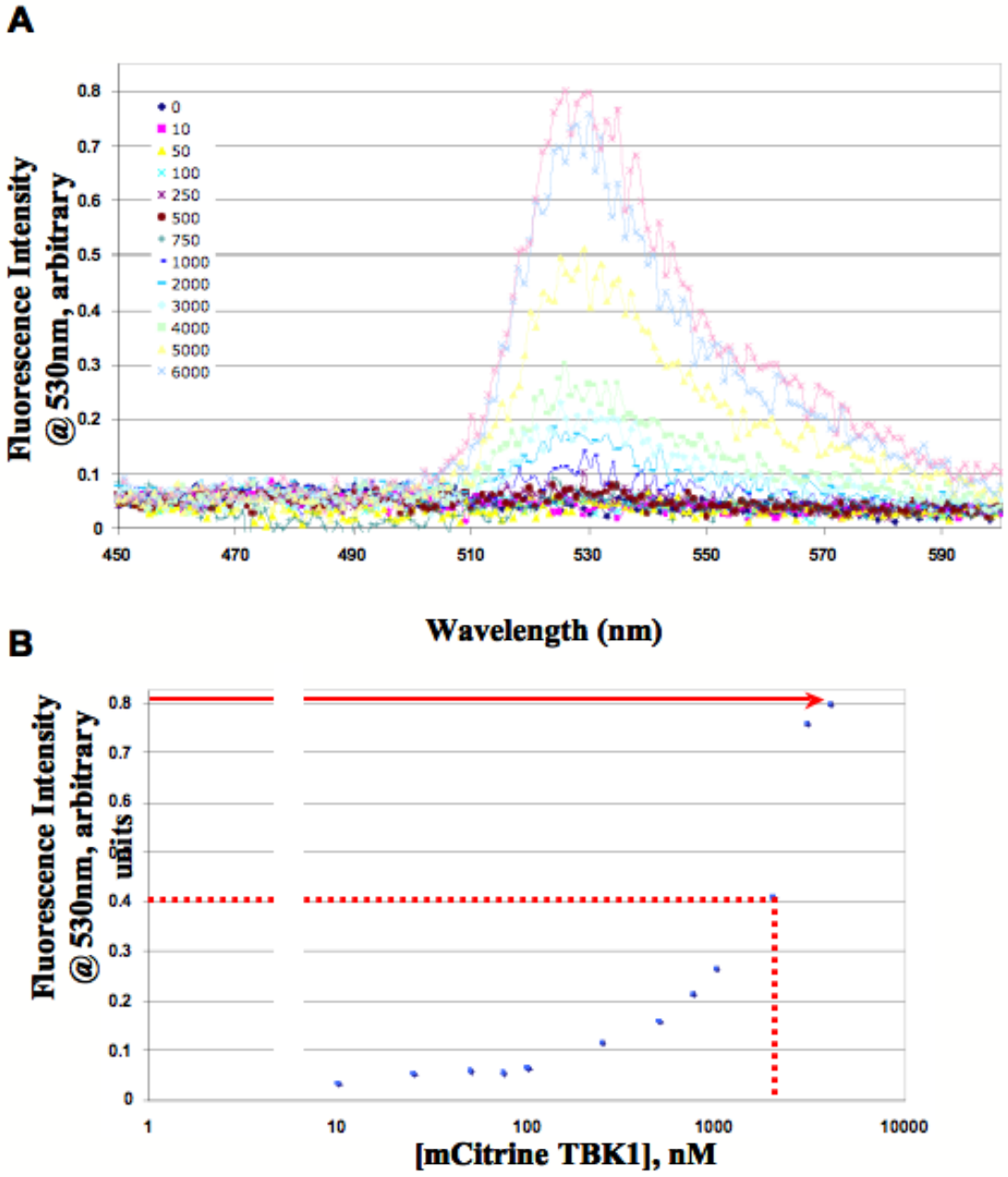

Figure 26. *Binding Curve showing µM binding of NAP1 KBD and TBK1 SBM* **A).** Graph showing the net emission spectra (exciting @ 430nm) from 'mCFP NAP1 KBD + mCitFP TBK1 SBM' and following emission from 450-600nm, with the concentration of mCFP NAP1 KBD held at 0.5µM and mCitFP TBK1 SBM increased from 0-6µM with wavelength (nm) on the x-axis and fluorescence intensity on the y-axis. **B)** Plot of binding curve with the concentration of mCitrine TBK1 (nM) on the x-axis and fluorescence intensity @ 530 nm on the y-axis was curve-fit to a 3-parameter sigmoidal equation gives a KD value of approximately 2 µM.

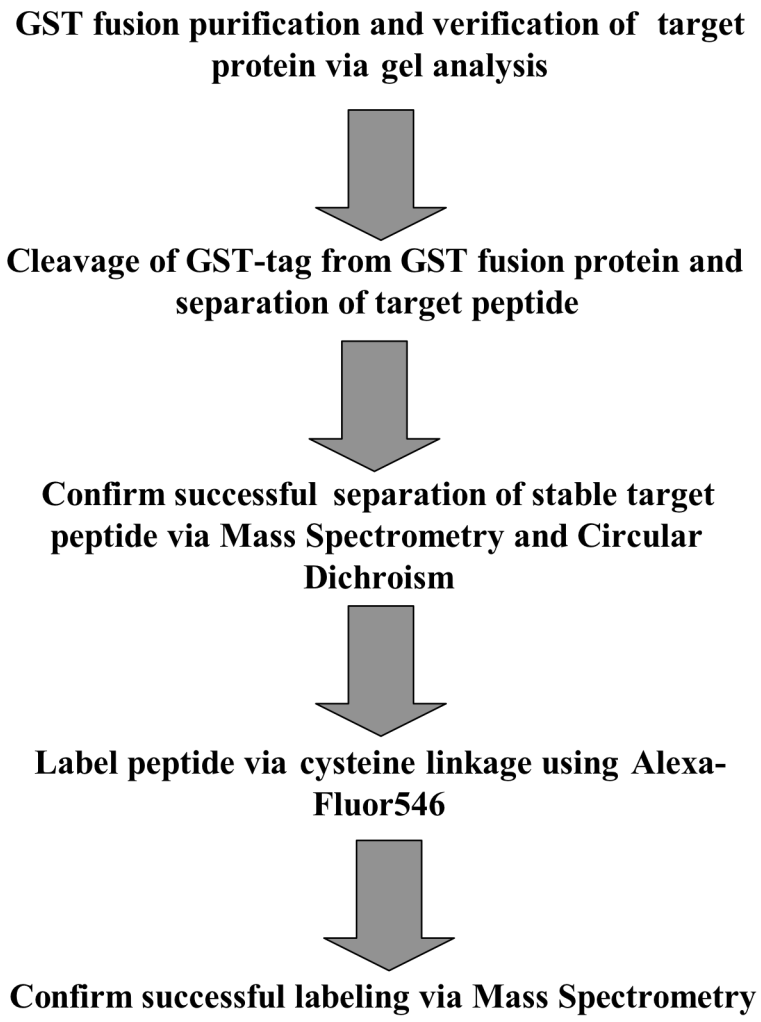

Figure 27. *Purification and verification of GST-IKK ε SBM peptide labeling.* Flowchart illustrating the process of purification and verification of successful AF546 labeling either the TBK1 or IKK ε SBM peptide.

3.4.2 NAP1 KBD-IKKε SBM Interactions

Alexa-Fluor 546-Labeling of IKKε SBM peptide

Successful purification of pure IKKε SBM was labeled with Alexa-Fluor 546 per manufacturer's protocol (Invitrogen) and following the diagram in Figure 27. No mutation was made, because a cysteine residue was already present at the N-terminus. Labeling occurs through disulfide-linkage between the thiol groups of the cysteine residue and the C5-malamide of the Alexa-Fluor.

Alexa-Fluor 546 (AF546), 1mg, is dissolved in 333μl of FRET buffer, for a final concentration of .33μM. AF546 is added at the 3X the concentration of the target peptide to label. FRET buffer is added for necessary dilutions. The reaction is allowed to go for 2 weeks at 4° Celsius and excess label is remove via a desalting column, 3x 3' spins @1500rpm. Successful labeling of peptide was assessed again via mass spectrometry (Figure 17C), for use in small-molecule FRET experiments.

Fluorescent properties of donor and acceptor

To determine where the spectral overlap occurs for this particular FRET pair, the acceptor, AF546 IKKε-SBM, was emit at 570nm and an excitation scan (from 300-565nm) and an emission scan (from 550-650nm), exciting at 520nm, were collected separately (Figure 28). The donor, mCFP NAP1 KBD, has already been characterized (Figure 22).

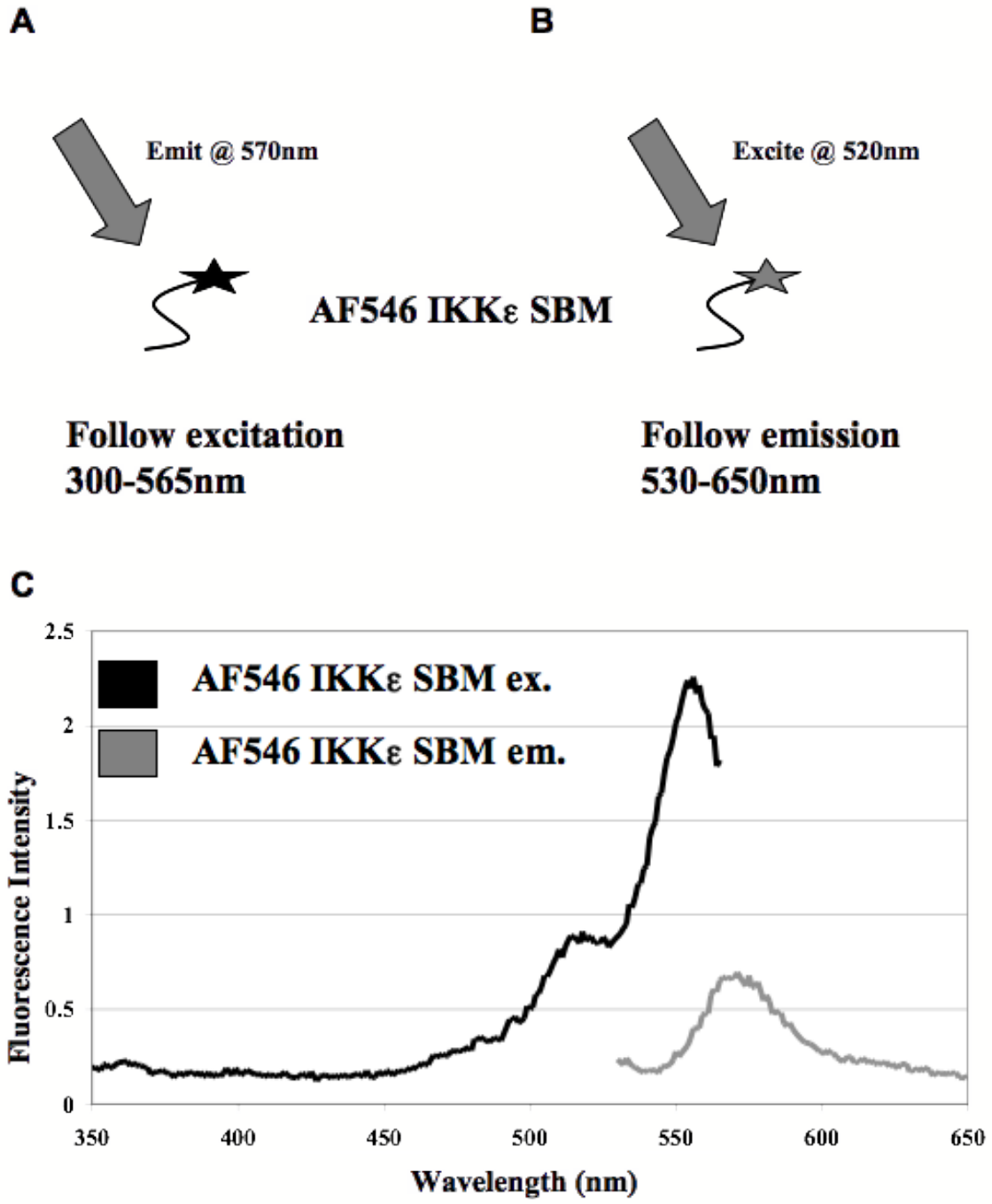

Figure 28. *Experimental design of FRET experiment.* Cartoon diagram of **A)** excitation and **B)** emission scans collected for AF546 IKKε SBM (687-709). **C)** Graph showing the experimental excitation and emission spectrum for AF546 IKKε SBM with wavelength (nm) on the x-axis and fluorescence intensity on the y-axis.

FRET experimental set-up (Ellis Bell)

Based on these spectra, the donor, mCFP NAP1 KBD, was excited at 430nm and emission spectra were collected (from 450nm to 650nm) to observe the interaction between mCFP NAP1 KBD and AF546 IKKε SBM (data not shown), to obtain optimal experimental results. A total of four scans were completed every 1nm for each concentration of the acceptor. A set amount of the acceptor, AF546 IKKε, at unknown concentration, was added to a cuvette and the donor, mCFP NAP1 KBD, was held titrated in, at concentrations ranging from 0-3 μM, large enough to observe FRET pairing. FRET buffer (20mM HEPES pH 7.5, 150mM NaCl, 1mM βME) was added to maintain constant volume in all cuvettes. Scans were performed after the addition of each aliquot of mCFP NAP1 KBD.

Again, non-specific interactions between the two fluorphores, mCFP and AF546 were corrected for. For this set-up, the same experiment was performed as for the experimental, however, no AF546 IKKε SBM was added and only buffer was in the cuvette to start and again mCFP NAP1 KBD was titrated in.

Data Analysis

This data was corrected by subtraction of the integrated area of the resonance energy transfer (RET) signal for the control spectra from the experimental spectra. The raw data was fit to a binding curve (integrated area of the RET signal vs. mCFP NAP1 KBD (μM)) where the K_D is approximately 1μM (Figure 29). This agrees with the NAP1 KBD-TBK1 SBM data, indicating that mCFP NAP1 KBD interacts with both the kinase's SBMs at low-micromolar affinity.

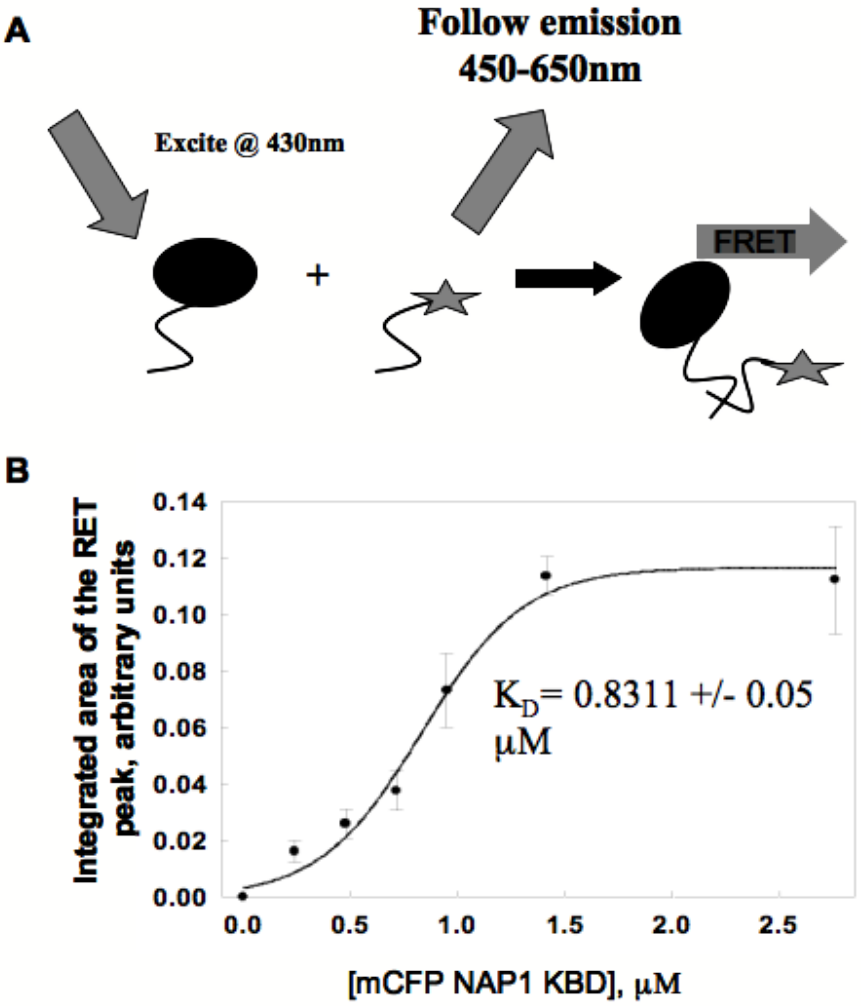

Figure 29. *Binding Curve showing mM binding of NAP1 KBD and IKKe SBM* **A).** Cartoon diagram illustrating the experimental emission spectrum for mCFP NAP1 KBD (black) and mCitFP TBK1 SBM (gray) and the range for following the emission **B)** Plot of binding curve with the concentration of mCFP NAP1 KBD (mM) on the x-axis and the Integrated area of the resonance energy transfer (RET) peak on the y-axis when fit to a three-parameter sigmoidal curve gives a KD value of 0.83 mM.

Data collected by Dr. E. Bell at University of Richmond, Richmond, VA.

Chapter 4. Discussion

The data shows that NAP1 protein domains form head-to-head dimers. Furthermore, homo-dimerization of the NAP1CC region may mediate homo-dimer formation of the NAP1 KBD, but more importantly is the hetero-interactions they form with the kinases' SBM. The CC domain region, as well as, NAP1's ability to behave as a dimer, may mediate NAP1 KBD's hetero-interactions with the kinase. This interaction has been shown to be necessary for IRF3 phosphorylation leading to production of type I IFNs.

It has previously been reported that the type I IFN pathway has a second scaffold protein, SINTBAD. Both the NAP1 and SINTBAD scaffold proteins, have a conserved site, specific for kinase, TBK1 and IKKε[1], recognition. NAP1 has also been shown to bind SINTBAD; questioning whether it functions independently with the kinases or with the aid of another scaffold protein(s)[1]. These protein-interaction domains are used to form large molecular weight protein interaction networks (PINs). In fact, both NAP1 and TBK1 were shown to be associated with high molecular weight complexes in TLR3 unstimulated HeLa cells[9]. In addition, both of these scaffold proteins have multiple predicted coiled-coil domains, which are rod-like alpha helices that are known to mediate protein-protein interactions. However, the mechanism behind the NAP1-TBK1 interaction, which is required for IRF3 phosphorylation leading to production of type I IFNs, is unknown. While all the FRET data was collected with mCFP NAP1 KBD in its monomeric state, it has not been determined if mCFP NAP1 KBD at dimeric concentrations would tighten hetero-interactions with the kinases. This work is currently ongoing.

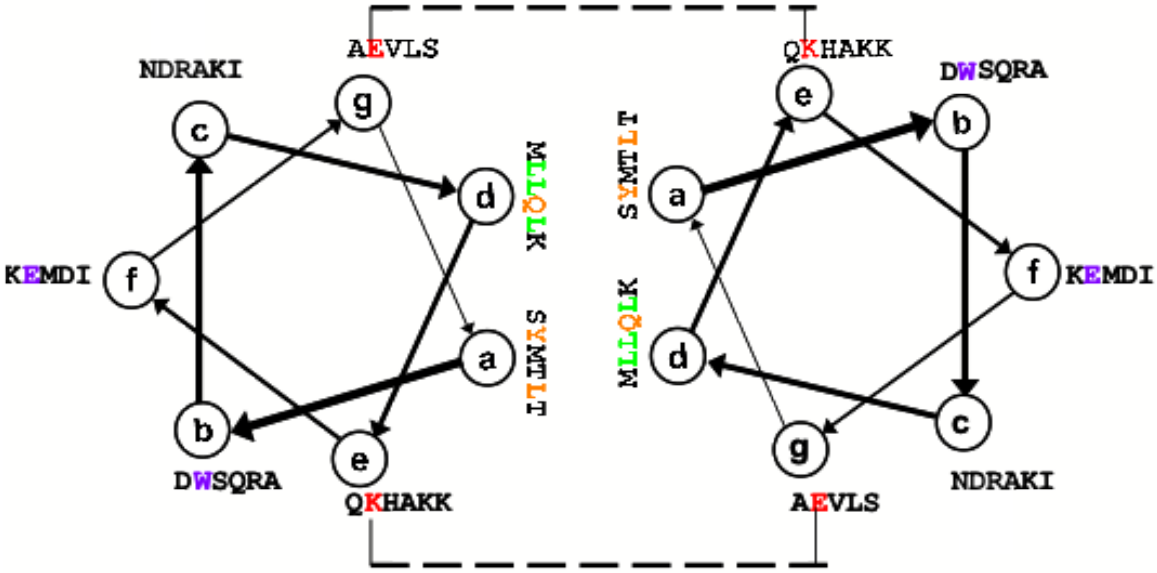

Figure 30. *Essential residues for NAP1 KBD dimer stability.* Helical wheel representation of NAP1 KBD (216–250 aa) is shown. Mutation sites that had a negative effect on kinase binding are highlighted in orange and mutation sites that had no effect are shown in purple. Possible mutations that may effect the stability of the dimer interface are highlighted in green. Lastly, mutations that may effect electrostatic interaction between the helices and further stabilize the dimer are highlighted in red.

As previously mentioned, the Randow group has identified some key residues that have diminished the scaffold-kinase binding, which are colored orange in the helical wheel representation (Figure 30). These residues are found on the dimer interface and necessary for stabilizing the hydrophobic core. Conversely, mutation sites that had no effect on kinase binding, because they lie outside the dimer interface, are colored purple (Figure 30). Therefore, it is possible that dimer formation may enhance and stabilize hetero-interactions with the kinases. Furthermore, polar amino acids have been shown to contribute to specificity of hetero-dimer formation by favoring associations with complementary polar groups. For example, Tyr-223 of the NAP1 KBD when mutated to Ala shows complete loss of NAP1-TBK1 interaction. No such residue was reported for IKKε.

Extensive studies of coiled-coil domains have shown that in the formation of a coiled-coil dimer that hydrophobic residues, particularily leucine residues, are found on one face of the dimer and buried in the interior, which forms a hydrophobic core stabilizing the dimer interaction. In fact, disruption of these leucine pairs even with other hydrophobic residues has lead to destabilization of the dimer. This agrees with the predicted residues we found from the NAP1 KBD model we built that may stabilize dimer formation.

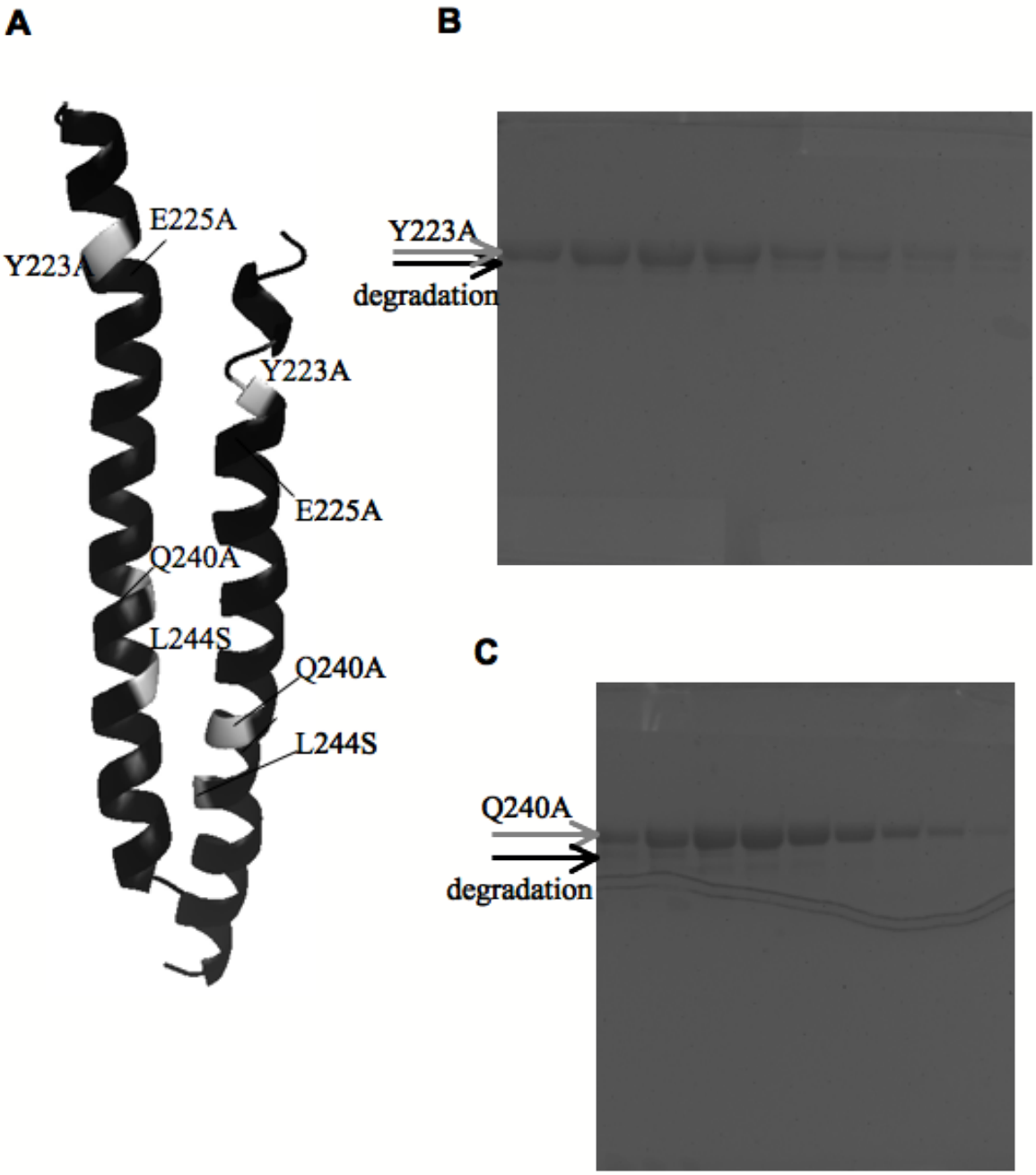

Figure 31. *Recombinant NAP1 KBD Expression of mutants.* **A)** The sites identified by Randow et al. to be essential (gray) or dispensable (black) for TBK1 binding were mapped to the NAP1 KBD dimer model A and shown in their stick figure configuration . Samples were run on 10% Bis-Acryl SDS-PAGE gels showing recombinant protein expression of mCFP NAP1 KBD mutants **B)** Y223A and **C)** Q240A from 1ml Ni-NTA Histrap fractions. Gray arrows indicate full-length protein expression and black arrows denote degradation of product and non-specific bands.

Quikchange mutagenesis kits (Stratagene) that employ standard molecular biology and polymerase chain reaction (PCR) techniques was performed, as per manufacturer's protocol, to mutate a few of these residues: Y223A, Q240A, L244S (and L226/233/247S), E225A and E229A. Mutagenesis has been completed for the following residues: Y223A, Q240A, L244S and E225A, highlighted in Figure 31A. The remaining mutations are ongoing.

Initial purification of the completed mutations has yielded poor results of pure and stable protein to use for future experiments (Figure 31B-C). However, purification of the L244S mutant yielded enough sample (~3mg/ml) to analyze the oligomeric state (Figure 32) by analysis over the S200 Tricorn column (in 20mM HEPES pH 7.5, 150mM NaCl, 1mM βME). The elution pattern indicates that it is eluting as mainly a monomeric species. However, this run would need to be repeated and additional concentrations tested to confirm. This data suggests that the leucine residues are indeed required for dimer stabilization. The rest of the leucines and other residues are currently being tested.

The previously described mutants will be assessed for dimeric structure using SEC and NAP1-Kinase interactions via FRET to further elucidate the NAP1-TBK1/IKKε trimeric complex formation in this protein-interaction network and more importantly its specificity in downstream signaling.

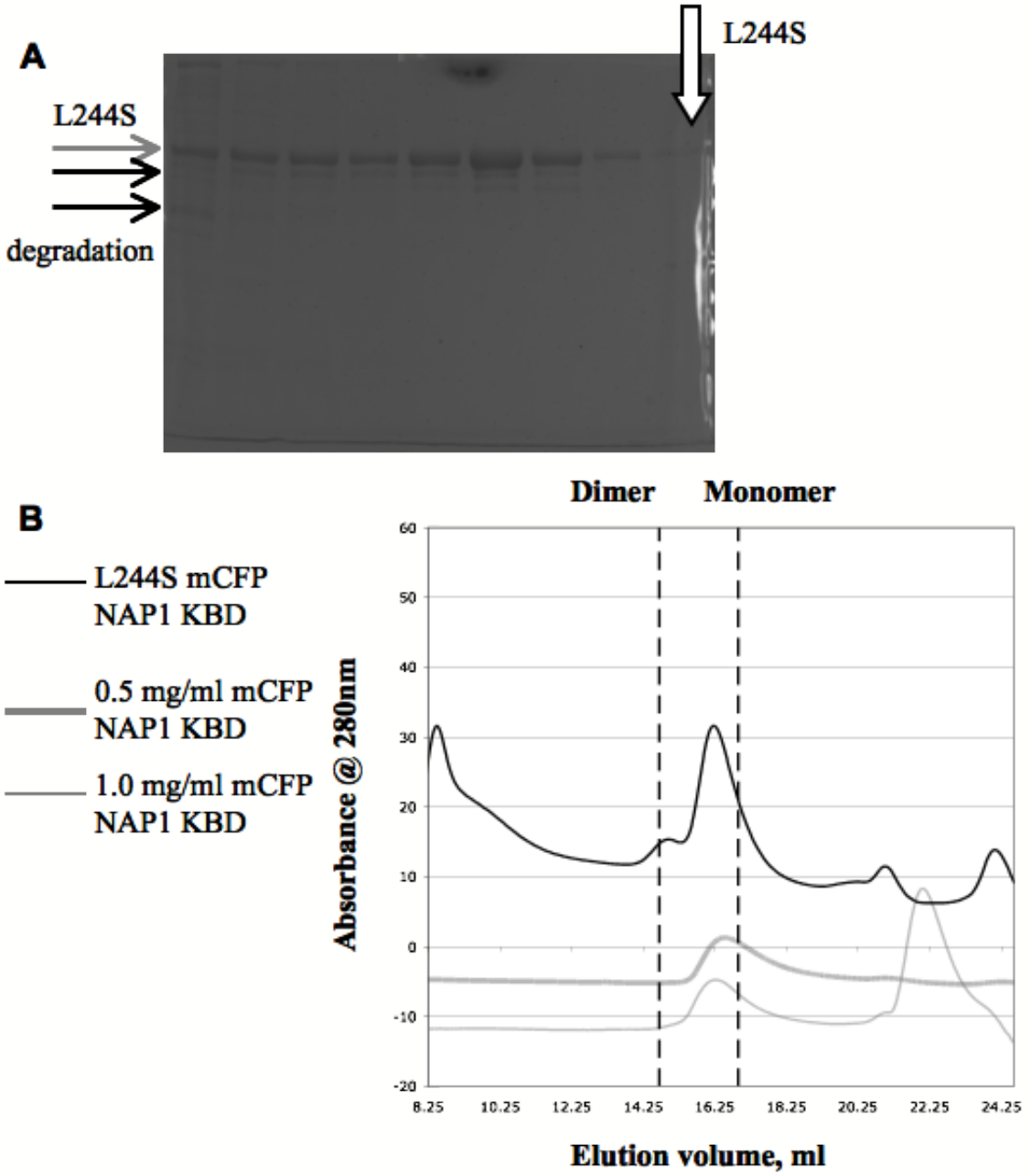

Figure 32. *Purification of NAP1 KBD L244S mutant.* **A)** Samples were run on 10% Bis-Acryl SDS-PAGE gels showing recombinant protein expression of mCFP NAP1 KBD L244S mutant from 1ml Ni-NTA Histrap fractions. Gray arrows indicate full-length protein expression and black arrows denote degradation of product and non-specific bands. **B)** mCFP NAP1 KBD L244S mutant, indicated by white arrow in part A, was separated on an S200 Tricorn Superdex size exclusion chromatography column, shown in black. At 1-2 mg/ml it elutes between a monomer and dimer. The elution volume for dimer and monomer mCFP NAP1 KBD are indicated by dashed lines. Oligomeric states were determined by comparison of elution patterns to globular, well-characterized gel filtration standards and 0.5mg/ml (thick gray line) and 1.0mg/ml (thin gray line) of mCFP NAP1 KBD WT.

Upon completion of mutagenesis, the mutated proteins will be assessed for dimeric structure using SEC and NAP1-Kinase interactions via FRET to further elucidate the NAP1-TBK1/IKKε role is this protein-interaction network and more importantly its role in mediating downstream signaling.

Literature Cited

1. Ryzhakov, G. and F. Randow, *SINTBAD, a novel component of innate antiviral immunity, shares a TBK1-binding domain with NAP1 and TANK.* EMBO J, 2007. **26**(13): p. 3180-90.
2. Jin, H., et al., *The VP35 protein of Ebola virus impairs dendritic cell maturation induced by virus and lipopolysaccharide.* J Gen Virol. **91**(Pt 2): p. 352-61.
3. Bowie, A.G. and L. Unterholzner, *Viral evasion and subversion of pattern-recognition receptor signalling.* Nat Rev Immunol, 2008. **8**(12): p. 911-22.
4. Janeway, C.A.T., P. Walport, M. Shlomchik, M.J., *Immuno-Biology; the immune system in health and disease*. 6th ed. 2005, New York: Garland Science. 823.
5. Paul, W.E., *Fundamental Immunology*. 5th Edition ed. 2003, Philadelphia: Lippincott, Williams & Wilkins. 1687.
6. Vercammen, E., J. Staal, and R. Beyaert, *Sensing of viral infection and activation of innate immunity by toll-like receptor 3.* Clin Microbiol Rev, 2008. **21**(1): p. 13-25.
7. Kandyil, R.M. and C.M. Davis, *Shellfish allergy in children.* Pediatr Allergy Immunol, 2009. **20**(5): p. 408-14; quiz 414.
8. Rushe, M., et al., *Structure of a NEMO/IKK-associating domain reveals architecture of the interaction site.* Structure, 2008. **16**(5): p. 798-808.
9. Fujita, F., et al., *Identification of NAP1, a regulatory subunit of IkappaB kinase-related kinases that potentiates NF-kappaB signaling.* Mol Cell Biol, 2003. **23**(21): p. 7780-93.
10. Huynh, Q.K., et al., *Kinetic mechanisms of IkappaB-related kinases (IKK) inducible IKK and TBK-1 differ from IKK-1/IKK-2 heterodimer.* J Biol Chem, 2002. **277**(15): p. 12550-8.